Supporting Information

Squaramide-Functionalized Coordination Capsule as Hydrogen-Bond-Donor Catalyst for Efficient Friedel-Crafts Alkylation

Contents

1. Experimental Section.

Materials and methods:

The ligand was synthesized following the literature methods (Figure S2).[1] All the chemicals and solvents were of reagent grade quality obtained from commercial sources and used without further purification.

Nuclear magnetic resonance:

^{1}H NMR spectra were recorded on Bruker spectrometers (400 MHz and 500 MHz), with chemical shifts referenced to the internal standard tetramethylsilane (TMS) at δ 0.0 ppm. ^{1}H DOSY spectra were measured on a Bruker 600MHz spectrometer.

Liquid chromatograph mass spectra:

ESI mass spectra were acquired on an Agilent G6224A HPLC-ESI-TOF/MS spectrometer, with acetonitrile/methanol as the mobile phase.

Liquid UV-Vis spectra:

Ultraviolet−Visible spectroscopy spectra were measured on a Shimadzu UV 2600 UV−Vis spectrophotometer.

High-performance liquid chromatography:

HPLC was performed on a SHIMADZU LC-2030 Plus system equipped with a ZORBAX SB-C18 column (250 × 4.6 mm I.D, s-5 μm) using methanol/water as mobile phase, to determine catalytic reaction yields.

Fluorescence spectra.

Fluorescence emission spectra of the solutions spectra were measured on an Edinburgh FLS1000 fluorescence spectrophotometer.

Single-Crystal X-ray diffraction

X-ray diffraction data were collected on a Bruker D8 Venture Photon II diffractometer with graphite monochromated GaKα (λ=1.34139 Å). An empirical

absorption correction using SADABS was applied for all data.[2] The structures were solved by the dual methods using the SHELXS program. All non-hydrogen atoms underwent anisotropic refinement by full matrix least-squares on F2 by the use of the program SHELXL,[3] and hydrogen atoms were included in idealized positions with thermal parameters equivalent to 1.2 times those of the atoms to which they were attached. Some remaining Q peaks could not be successfully resolved despite numerous attempts at modeling, and consequently the SQUEEZE function of PLATON was used to account for these highly disordered solvents.[4] All non-hydrogen atoms underwent anisotropic refinement. Hydrogen atom positions were calculated geometrically**.**

Synthesis of Ligand

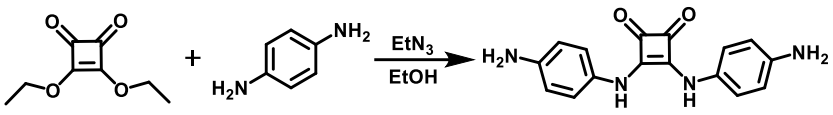

Figure S1 Synthesis of ligand L

Synthesis of ligand L:

Diethyl squarate (1.08 mL, 7.3 mmol), p-phenylenediamine (1.59 g, 14.7 mmol), and triethylamine (10.24 mL) were dissolved in 50 mL of ethanol. The reaction mixture was stirred at 60 ℃ for 24 h. The resulting precipitate was collected by filtration while hot, washed with ethanol and diethyl ether, and subsequently dried in vacuo to afford L as a brown solid. Yield: 1.9 g (88%). **^{1}H NMR (500 MHz, DMSO-*d6*)** δ 9.43 (s, 2H), 7.15 (d, J = 8.2 Hz, 4H), 6.56 (d, J = 8.6 Hz, 4H), 5.00 (s, 4H).

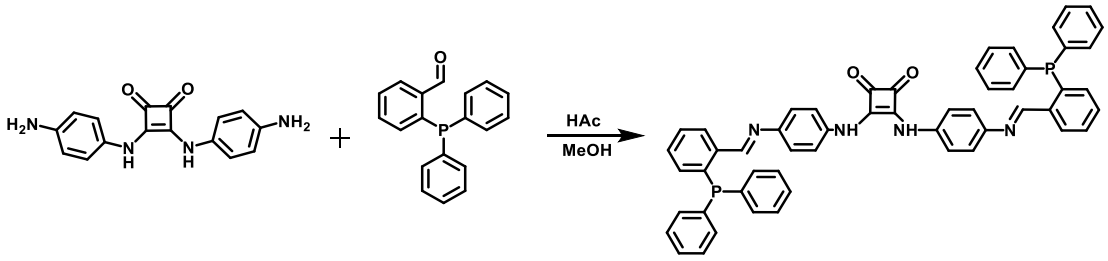

Figure S2 Synthesis of ligand L1

Synthesis of ligand L1:

Ligand L (0.59 g, 2.0 mmol) and 2-diphenylphosphinobenzaldehyde (1.16 g, 4.0 mmol) were added to 60 mL of acetonitrile. Glacial acetic acid (15 drops) was slowly added dropwise to the mixture under continuous stirring. The reaction mixture was then heated to reflux at 80°C for 24 h. The resulting solid was collected by filtration while hot, washed sequentially with methanol and diethyl ether, and dried in vacuo to afford L1 as a pale yellow powder. Yield: 1.42 g (85%). **^{1}H NMR (400 MHz, DMSO-*d6*)** δ 9.99 (s, 2H), 9.01 (d, *J* = 4.8 Hz, 2H), 8.10 (d, *J* = 6.5 Hz, 2H), 7.55 (d, *J* = 7.6 Hz, 2H), 7.47-7.39 (m, 18H), 7.26 (dt, *J* = 8.3, 4.3 Hz, 8H), 6.99 (d, *J* = 8.2 Hz, 4H), 6.89-6.83 (m, 2H).

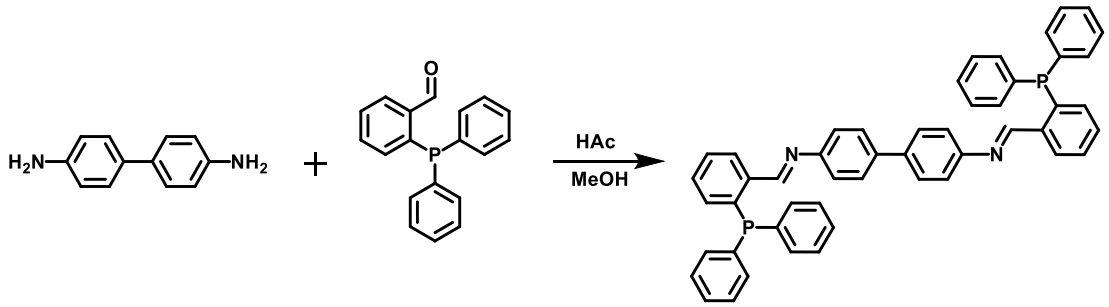

Figure S3 Synthesis of ligand L2

Synthesis of L2:

Benzidine (0.37 g, 2.0 mmol) and 2-diphenylphosphinobenzaldehyde (1.17 g, 4.0 mmol) were dissolved in 60 mL of methanol in a 100 mL round-bottom flask, followed by the addition of glacial acetic acid (1 mL). The reaction mixture was heated to reflux at 80°C for 24 h. The precipitated solid was collected by filtration while hot, washed with methanol, and dried at 80°C to afford ligand L2 as a yellow solid. Yield: 88.7%. **^{1}H NMR (400 MHz, $CDCl_3$)** δ 9.14 (d, *J* = 5.3 Hz, 2H), 8.25 (dd, *J* = 8.0 Hz, 2H), 7.54 (d, *J* = 8.1 Hz, 4H), 7.48 (d, *J* = 7.6 Hz, 2H), 7.39 (d, *J* = 5.4 Hz, 16H), 7.35 (s, 4H), 7.31-7.27 (m, 2H), 7.00 (d, *J* = 8.1 Hz, 4H), 6.96 (t, *J* = 6.1 Hz, 2H).

Synthesis of macrocycle H1:

Ligand L1 (83.8 mg, 0.1 mmol) and $Pd(CH_3CN)_4(BF_4)_2$ (46.3 mg, 0.104 mmol) were added to 45 mL of freshly distilled acetonitrile. The reaction mixture was degassed under vacuum and backfilled with nitrogen three times, and subsequently stirred at 60°C for 24 h under a nitrogen atmosphere. The resulting purple solution was filtered through an organic membrane filter. Slow diffusion of diethyl ether into the filtrate over one week afforded red crystals. Yield: 40% (based on ligand L1). **^{1}H NMR (500 MHz, DMSO-*d*$_6$)** δ 10.28 (s, 2H), 8.74-8.64 (m, 2H), 8.52 (s, 2H), 8.01 (s, 12H), 7.75-7.68 (m, 6H), 7.62 (d, J = 9.3 Hz, 6H), 7.49 (d, J = 8.4 Hz, 6H), 7.21 (t, J = 9.4 Hz, 4H). **^{13}C NMR (126 MHz, DMSO-*d*$_6$)** δ 170.82, 166.49, 166.16, 141.94, 141.69, 140.38, 138.52, 135.94, 135.11, 134.55, 134.27, 133.19, 132.00, 130.38, 129.58, 129.48, 125.52,

123.23, 122.76, 118.55, 60.23, 21.24, 14.56.

Synthesis of compound H2:

Ligand L2 (72.8 mg, 0.1 mmol) and $Pd(CH_3CN)_4(BF_4)_2$ (46.3 mg, 0.104 mmol) were added to 45 mL of freshly distilled acetonitrile. The reaction mixture was degassed under vacuum and backfilled with nitrogen three times, and subsequently stirred at 60°C for 24 h under a nitrogen atmosphere. The resulting yellow solution was filtered through an organic membrane filter. Slow diffusion of diethyl ether into the filtrate over one week afforded yellow crystals. Yield: 35% (based on ligand L2). **^{1}H NMR (500 MHz, DMSO-*d*$_6$)** δ 8.72 (d, *J* = 12.9 Hz, 2H), 8.56 (s, 2H), 7.98-7.86 (m, 12H), 7.78 (d, *J* = 13.8 Hz, 8H), 7.66 (t, *J* = 7.3 Hz, 4H), 7.52 (t, *J* = 7.4 Hz, 4H), 7.27 (t, *J* = 9.4 Hz, 4H), 7.00 (s, 2H).

Synthesis of compound M1:

N,N-Dimethyl-1,4-phenylenediamine (13.5 mg, 0.1 mmol), 2-diphenylphosphinobenzaldehyde (29.0 mg, 0.1 mmol), and $Pd(CH_3CN)_4(BF_4)_2$ (46.3 mg, 0.104 mmol) were added to 45 mL of acetonitrile. The reaction mixture was degassed under vacuum and backfilled with nitrogen three times, and subsequently stirred at 60°C for 24 h under a nitrogen atmosphere.**^{1}H NMR (500 MHz, CD$_3$CN)** δ 8.09 (d, J = 12.8 Hz, 1H), 7.91 (t, J = 7.5 Hz, 1H), 7.84 (dd, J = 7.5, 3.9 Hz, 1H), 7.81-7.64 (m, 5H), 7.55 (td, J = 7.8, 2.5 Hz, 2H), 7.43 (t, J = 7.5 Hz, 1H), 7.32 (d, J = 8.8 Hz, 2H), 7.24-7.03 (m, 3H), 6.49 (d, J = 8.7 Hz, 3H), 3.03 (s, 6H).

General procedure for Friedel-Crafts alkylation reactions：

All catalytic reactions were conducted in a pressure tube. β-nitrostyrene (0.05 mmol), indole (0.075 mmol), and 2.5 μmol of H1 were mixed in 2 mL of dichloromethane. The reaction was allowed to proceed at 60 ℃ for 24 h. The yields of the products were determined by HPLC analysis performed on a SHIMADZU LC or by ^{1}H NMR spectroscopy using 1,3,5-trimethoxybenzene as an internal standard.

2. Single Crystal X-ray Crystallography

Table S1. Crystal data and structure refinement of H1.

Compound	H1
Empirical formula	$C_{118}H_{101}F_{18}N_{11}O_{10}P_7Pd_2$
Formula weight	2604.68
Temperature [K]	150.00
Crystal system	triclinic
Space group (number)	$P\bar{1}$ (2)
a [Å]	14.9048(19)
b [Å]	21.474(3)
c [Å]	26.501(3)
α [°]	110.495(5)
β [°]	100.234(6)
γ [°]	97.695(7)
Volume [Å^3]	7639.7(16)
Z	2
ρ_{calc} [gcm^{-3}]	1.132
μ [mm^{-1}]	2.172
F(000)	2650
Crystal size [mm^3]	0.22×0.32×0.36
Radiation	GaKα (λ=1.34139 Å)
2θ range [°]	5.93 to 105.96 (0.84 Å)
Index ranges	$-17 \le h \le 17$ $-25 \le k \le 25$ $-31 \le l \le 31$
Reflections collected	239152
Independent reflections	26433[R_{int} = 0.1392, R_{sigma} = 0.0971]
Data / Restraints / Parameters	26433 / 2669 / 1134
Absorption correction	0.4878 / 0.7050
T_{min}/T_{max}(method)	(multi-scan)
Goodness-of-fit on F^2	1.041
Final *R* indexes	R_1 = 0.1371
[$I \ge 2\sigma(I)$]	wR_2 = 0.3073
Final *R* indexes	R_1 = 0.1830
[all data]	wR_2 = 0.3421
Largest peak/hole [eÅ^{-3}]	0.69/−0.91
CCDC number	2539662

Table S2. Crystal data and structure refinement of H2.

Compound	H2
Empirical formula	$C_{245}H_{257}B_8F_{32.03}N_{23}O_{14.94}P_8Pd_4$
Formula weight	5131.16
Temperature [K]	170(2)
Crystal system	triclinic
Space group (number)	$P\bar{1}$ (2)
a [Å]	22.1764(10)
b [Å]	23.4544(11)
c [Å]	25.8084(13)
α [°]	84.514(2)
β [°]	76.721(2)
γ [°]	85.997(2)
Volume [Å^3]	12989.2(11)
Z	2
ρ_{calc} [gcm^{-3}]	1.312
μ [mm^{-1}]	2.291
F(000)	5280
Crystal size [mm^3]	0.250×0.320×0.350
Radiation	GaK_α (λ=1.34138 Å)
2θ range [°]	3.30 to 106.58 (0.84 Å)
Index ranges	$-26 \le h \le 26$ $-28 \le k \le 28$ $-30 \le l \le 30$
Reflections collected	350998
Independent reflections	45859[R_{int} = 0.0619 R_{sigma} = 0.0231]
Data / Restraints / Parameters	45859 / 7 / 2363
Absorption correction	0.6443 / 0.7310
T_{min}/T_{max}(method)	(multi-scan)
Goodness-of-fit on F^2	1.033
Final *R* indexes	R_1 = 0.0709
[$I \ge 2\sigma(I)$]	wR_2 = 0.2015
Final *R* indexes	R_1 = 0.0829
[all data]	wR_2 = 0.2144
Largest peak/hole [eÅ^{-3}]	1.60/−0.80
CCDC number	2539666

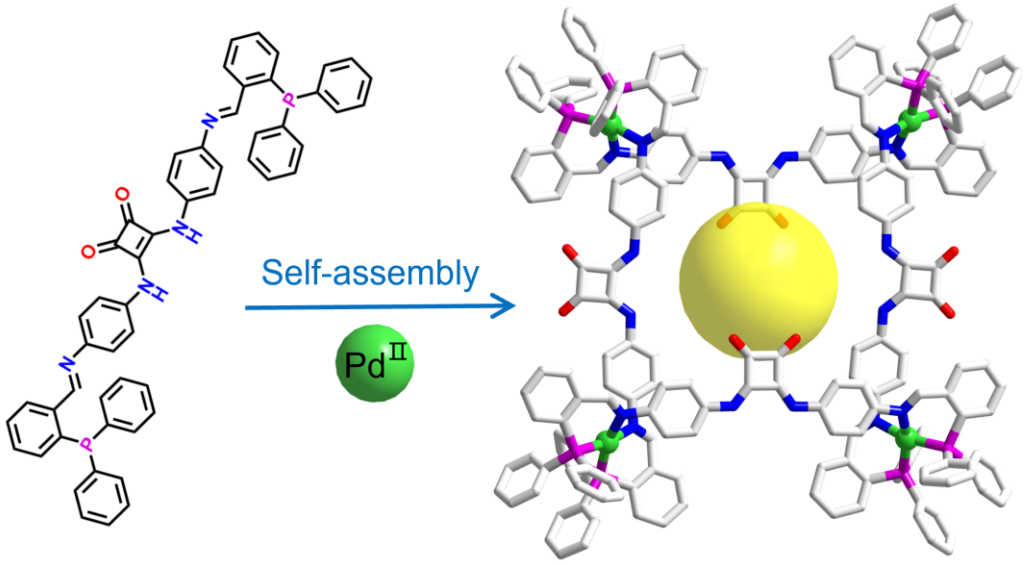

Figure S4. The self-assembly process of H1 and the inner cavity (yellow balls), where palladium, nitrogen, oxygen and phosphoru atoms are shown in green, blue, red and purple, respectively.

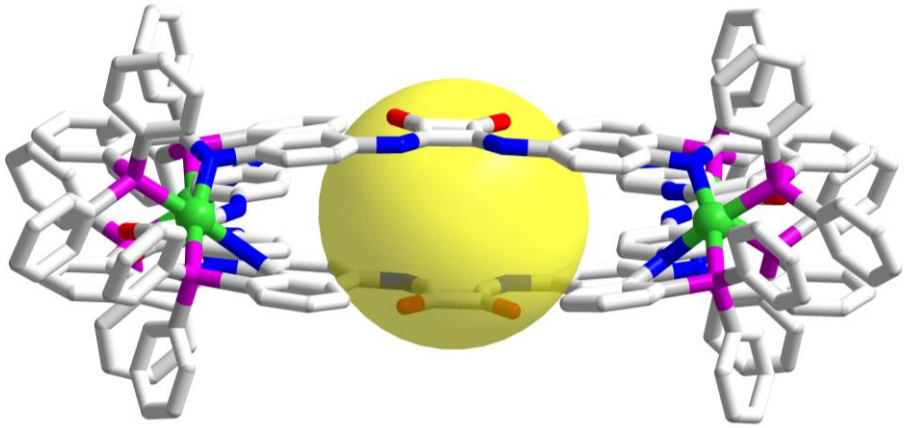

Figure S5. The cavity constructed by H1, its approximate radius is 4.2 Å.

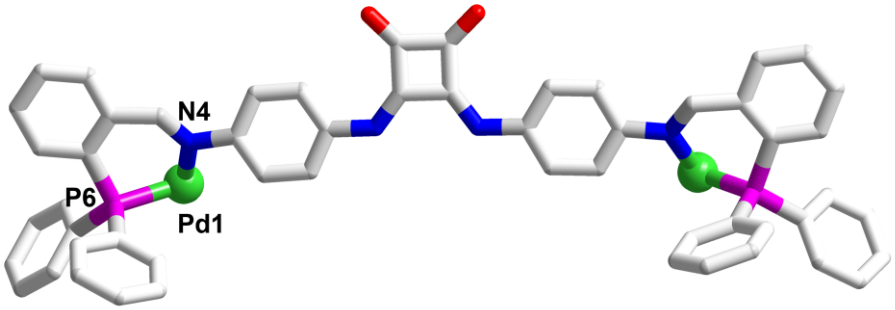

Figure S6. Molecular structure of H1 within a unique asymmetric unit, showing the backbone of the ligand in the complex. Selected bond distances (Å): Pd1-N4 2.0954(2), Pd1-P6 2.2609(3).

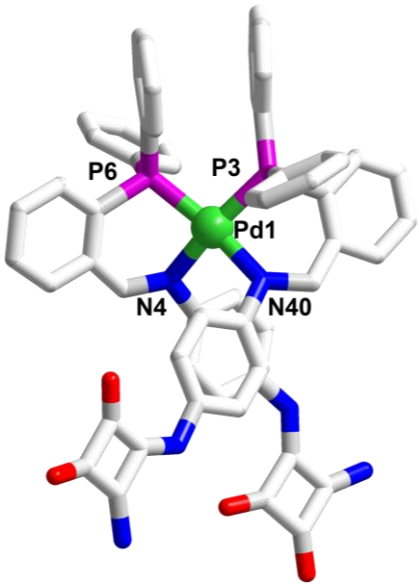

Figure S7. Coordination geometry of the Pd atom in H1. Selected angles (°): P6-Pd1-N4 86.575(13), P6-Pd1-P3 98.679(13), P3-Pd1-N40 86.981(13), N40-Pd1-N4 89.489(13).

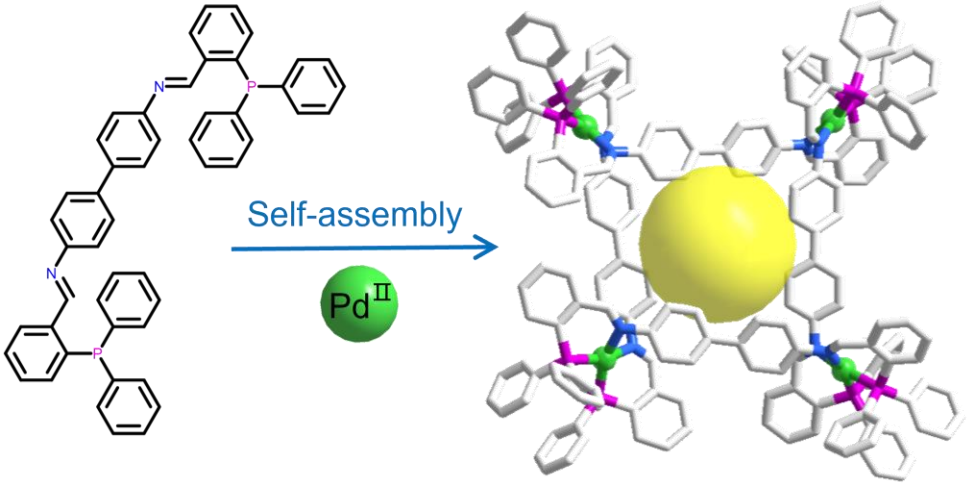

Figure S8. The self-assembly process of H2 and the inner cavity (yellow balls), where palladium, nitrogen and phosphoru atoms are shown in green, blue and purple, respectively.

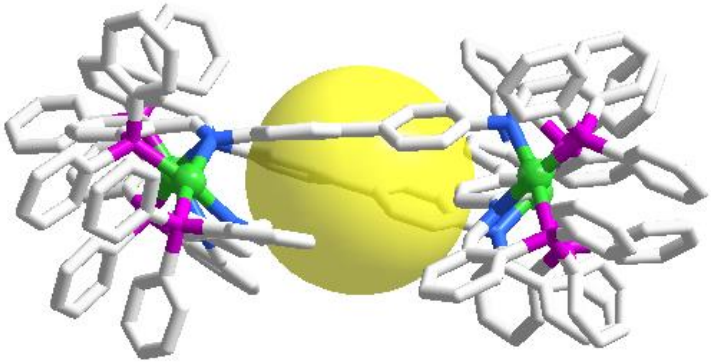

Figure S9. The cavity constructed by H2, its approximate radius is 3.8 Å.

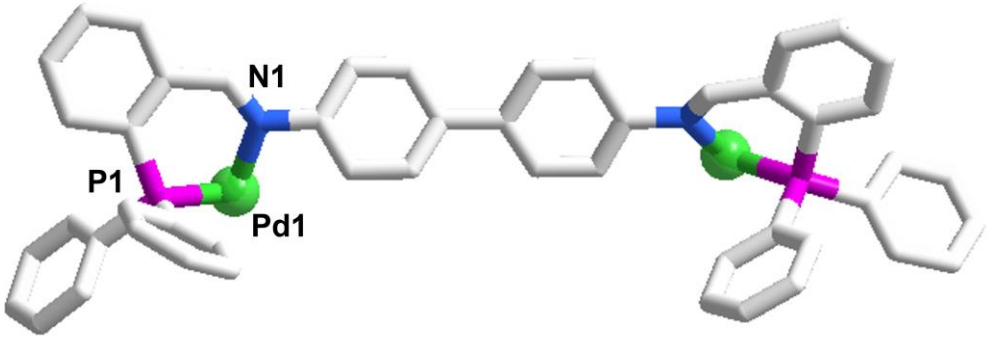

Figure S10. Molecular structure of H2 within a unique asymmetric unit, showing the backbone of the ligand in the complex. Selected bond distances (Å): Pd1-N1 2.078(15), Pd1-P1 2.247(4).

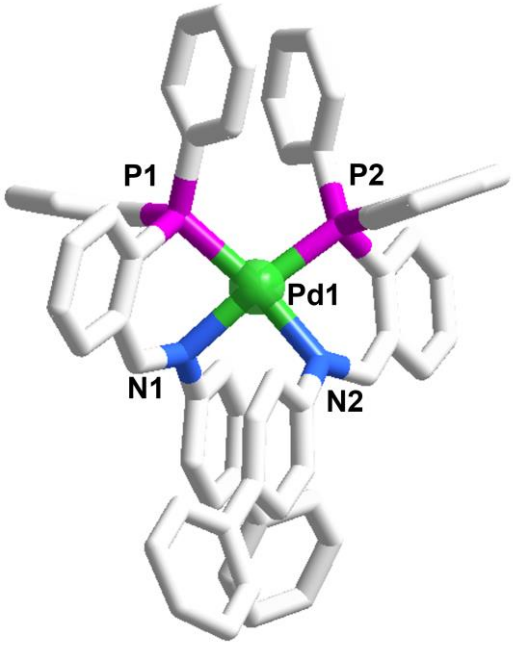

Figure S11. Coordination geometry of the Pd atom in H2. Selected angles (°): P1-Pd1-N1 84.4(4), P1-Pd1-P2 103.15(14), P2- Pd1-N2 87.4(5), N2-Pd1-N1 88.9(6).

3. Experimental Details.

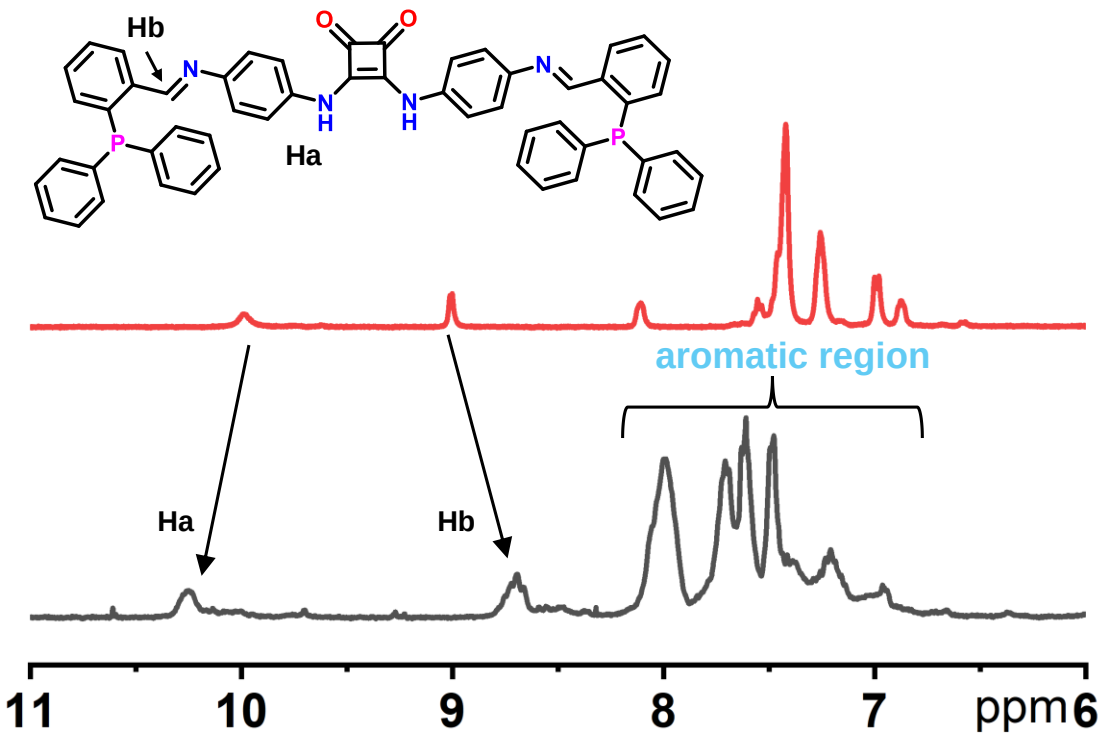

Figure S12. ^{1}H NMR (500 MHz, DMSO-d_6, 298K) spectrum of H1 (black line) and L2 (red line).

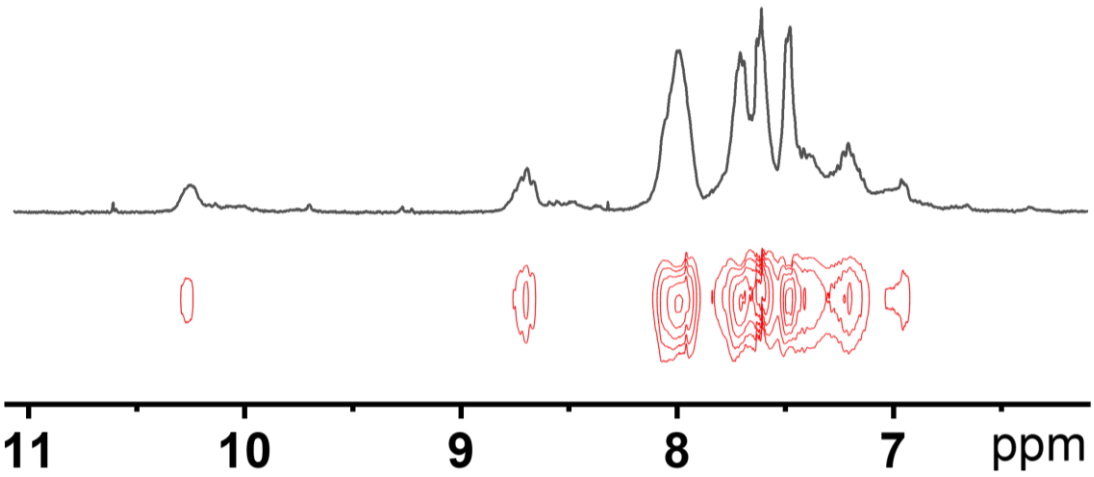

Figure S13. The ^{1}H DOSY spectrum of H1 (600 MHz, DMSO-d_6, 298K). The diffusion coefficient is 3.16×10^{-10} $m^2 \cdot s^{-1}$ in this solution.

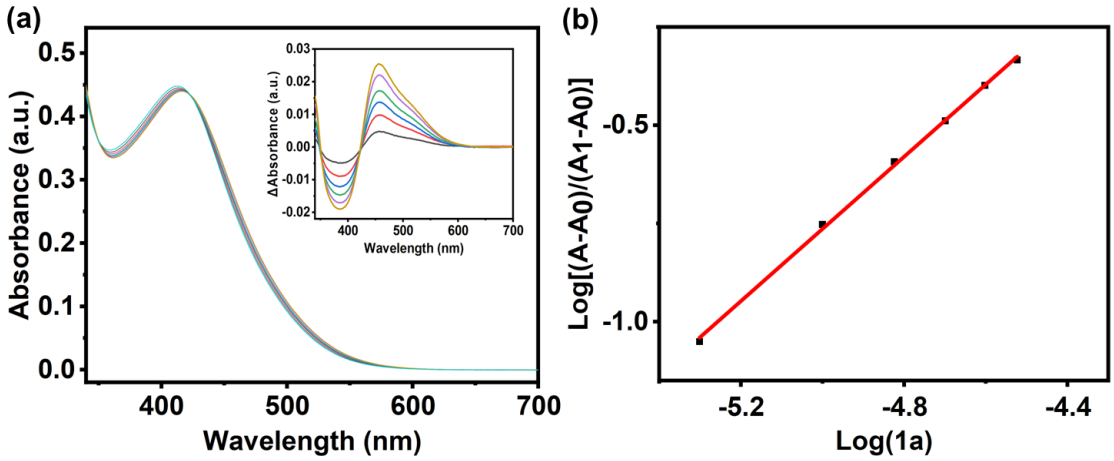

Figure S14. (a) UV-Vis spectra and difference spectra of the H1 (5 μM) upon the addition of furfural in an acetonitrile solution. (b) The linear fitting of the titration curve (recorded absorption at 460 nm), showing a 1:1 host-guest binding stoichiometry between H1 and 1a with an association constant calculated as 4.54×10^4 M^{-1}.

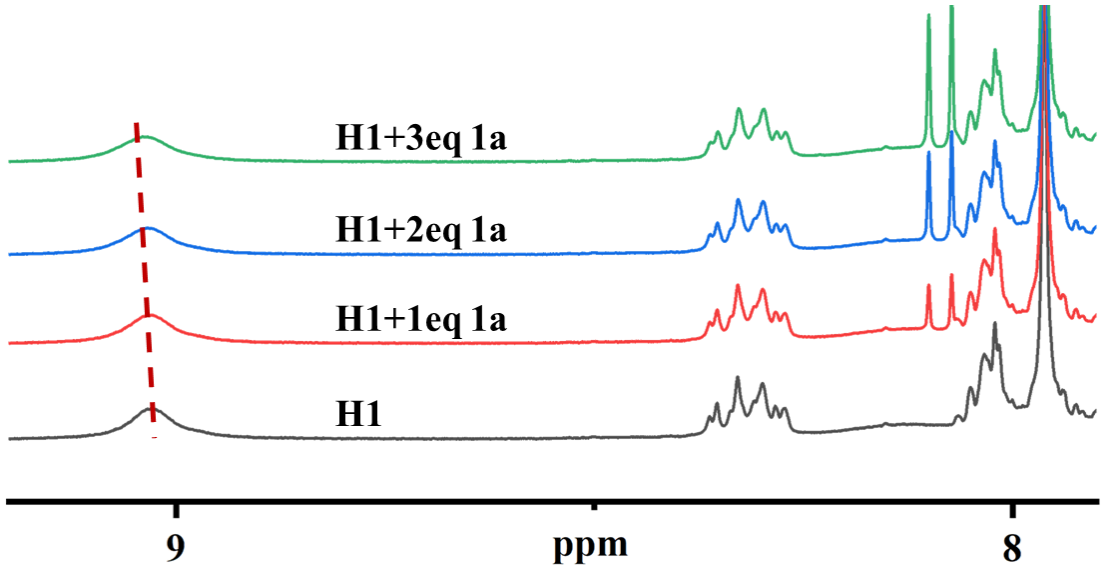

Figure S15. ^{1}H NMR (500 MHz, CD_3CN, 298K) titration of H1 (1.0 mM) upon the addition of 1a in CD_3CN.

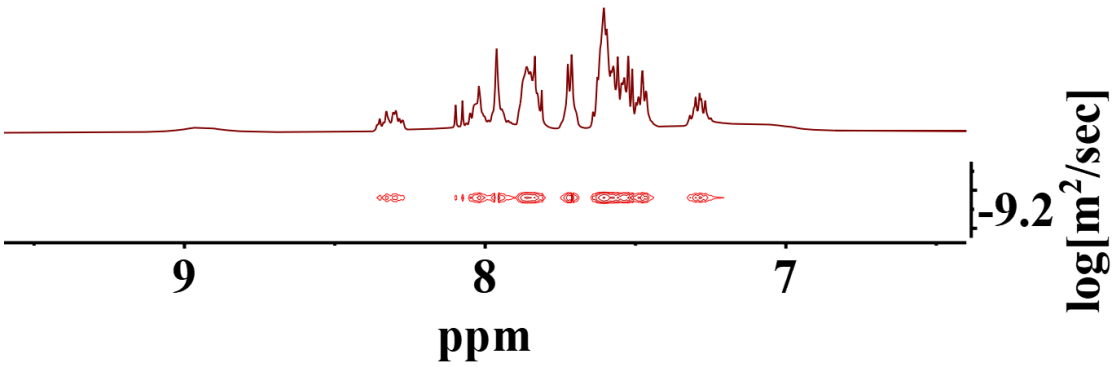

Figure S16. ^{1}H DOSY (600 MHz, CD_3CN, 298K) of the host-guest mixture of H1 and 1a. The diffusion coefficient is 9.1×10^{-10} $m^2 \cdot s^{-1}$ in this solution.

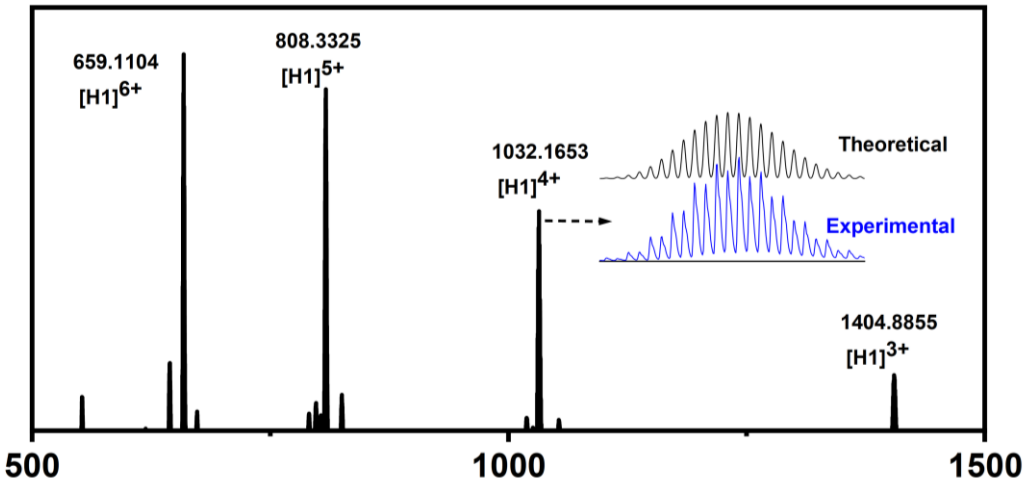

Figure S17. The ESI-MS spectrum of H1 (1 mM) in CH_3CN solution. The inserts show the measured and simulated isotopic patterns at *m/z* = 1032.1653.

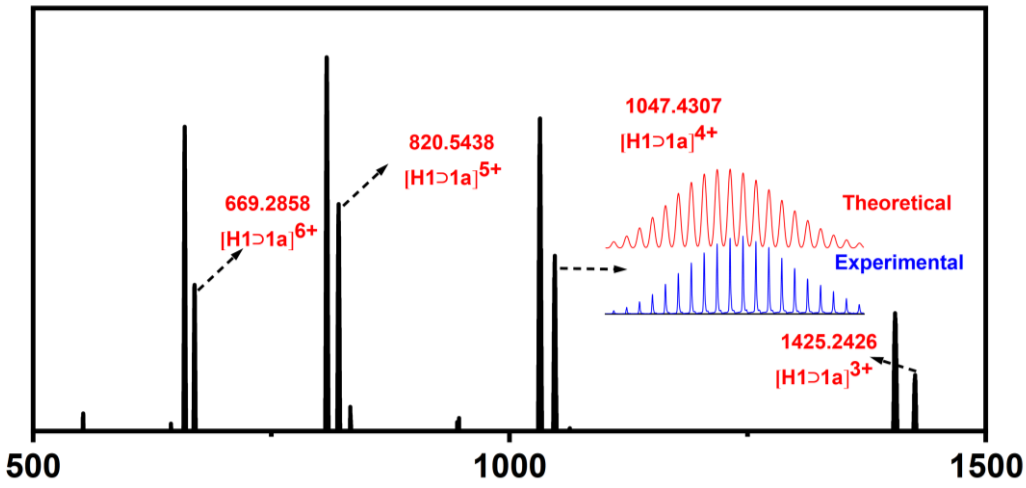

Figure S18. The ESI-MS spectrum of H1 (1 mM), β-nitrostyrene (3 mM) in CH_3CN solution. The inserts show the measured and simulated isotopic patterns of the host-guest mixture at *m/z* = 1047.4307.

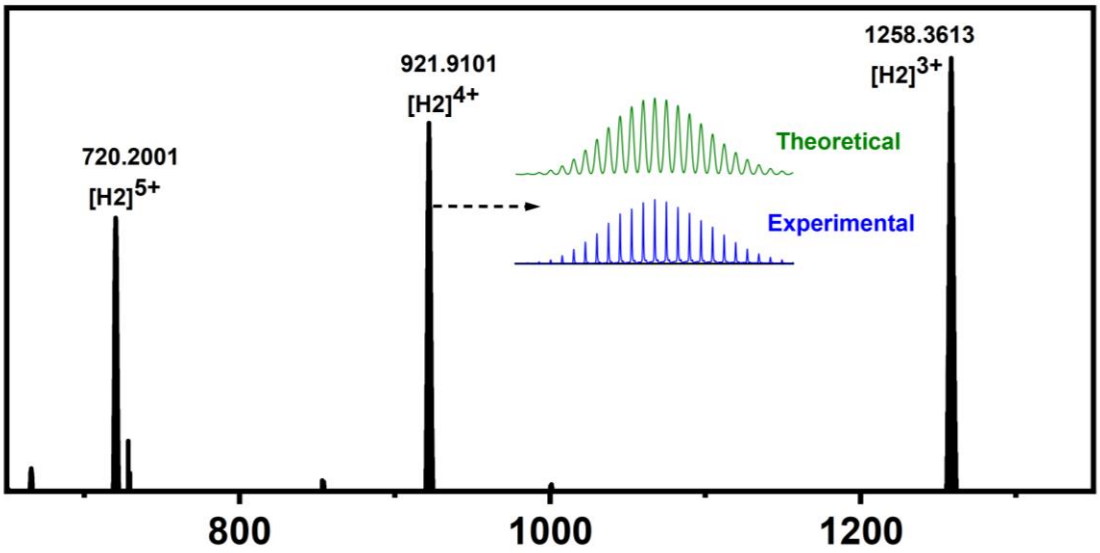

Figure S19. The ESI-MS spectrum of H2 (1 mM) in CH_3CN solution. The inserts show the measured and simulated isotopic patterns at *m/z* = 921.9101.

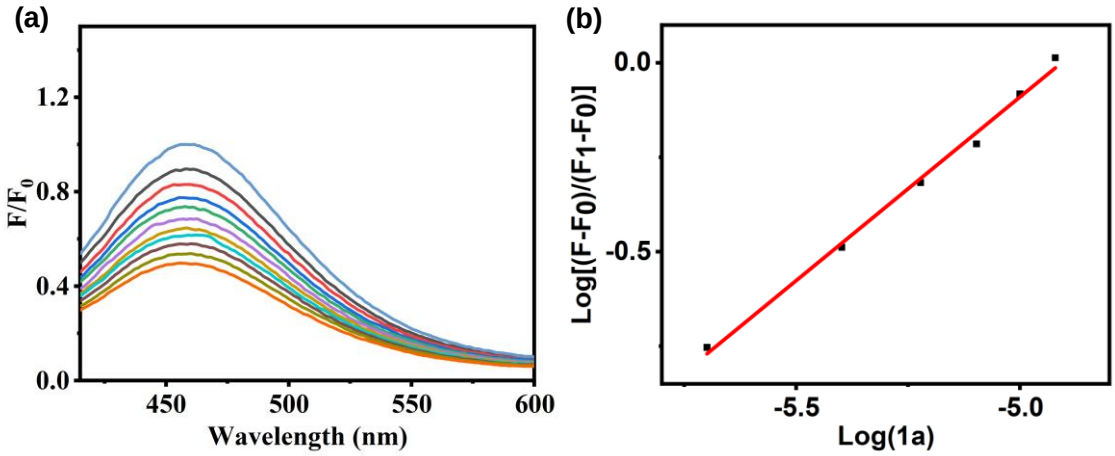

Figure S20. (a) The emission spectra of H1 (0.01 mM) upon addition of 1a. (b) The linearity fitting of the titration curve showing a 1:1 host-guest behavior between H1 and 1a with a constant of 4.61×10^4 M^{-1}.

Table S3. Optimization of Reaction Conditions.

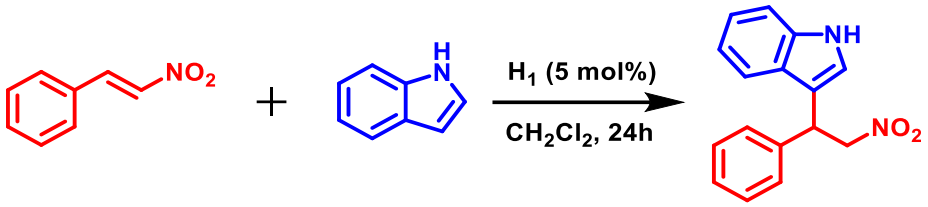

Entry	Deviation from standard conditions	Yield (%)
1[a]	none	63
2	3 mol%	50
3	10 mol%	60
4	MeOH replace CH_2Cl_2	16
5	DMSO replace CH_2Cl_2	10
6	No H1	trace
7[b]	$Pd(CH_3CN)_4(BF_4)_2$	trace
8[c]	Ligand L1	20
9	H2 replace H1	8
10	M1 replace H1	trace
11[d]	ATP-Na	34

[a]Standard conditions: β-nitrostyrene (0.05 mmol), indole (0.075 mmol), and H1 (5 mol%, 2.5 μmol) in CH_2Cl_2 (2 mL) at 60°C for 24 h. [b]Control experiment using $Pd(CH_3CN)_4(BF_4)_2$ to replace H1. To maintain the identical metal concentration, the addition of $Pd(CH_3CN)_4(BF_4)_2$ was 20 mol%. [c]Control experiment using L1 to replace H1. To maintain the ligand L1 concentration, the addition of L1 was 20 mol%. [d]25μmol ATP-Na was added as an inhibitor for the catalytic reaction. The yields were determined by ^{1}H NMR using 1,3,5-trimethoxybenzene as internal standard.

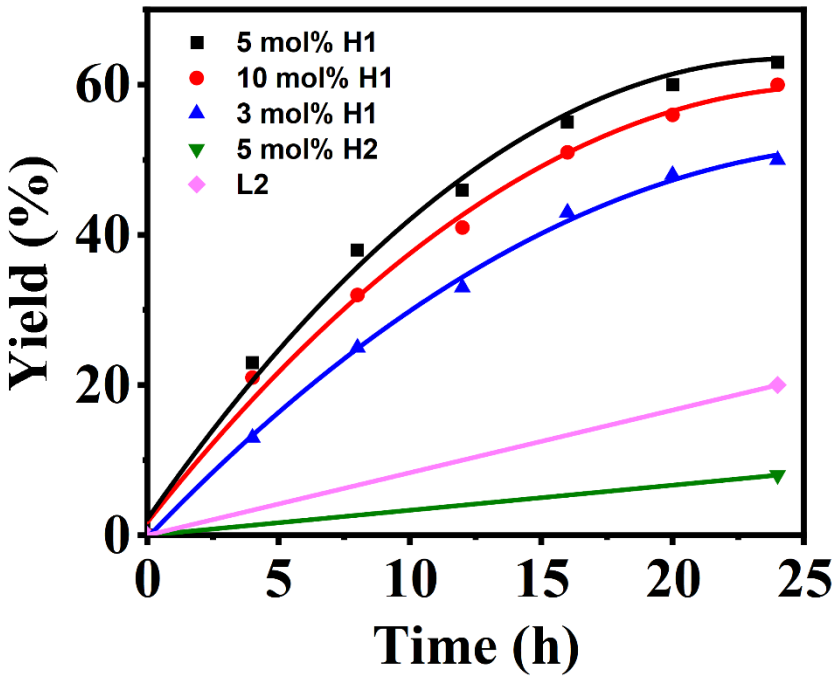

Figure S21. Reaction kinetics of the Friedel-Crafts alkylation with different loadings of catalyst H1 (and control groups).

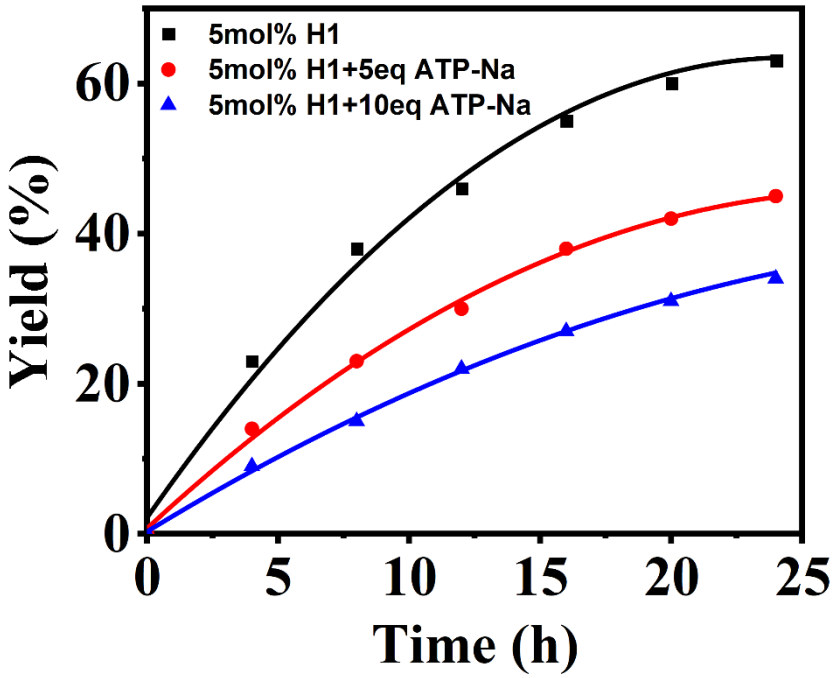

Figure S22. Reaction kinetics of the Friedel-Crafts alkylation in the presence of different equivalents of ATP-Na as a competitive inhibitor.

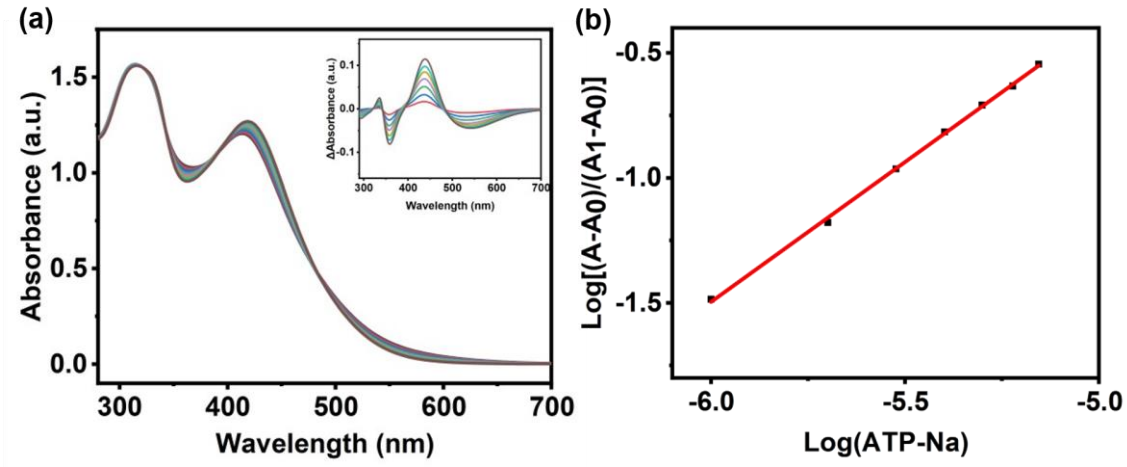

Figure S23. (a) UV-Vis spectra of the H1 (5 μM) upon the addition of ATP-Na in an acetonitrile solution. (b) linear fitting of the titration curve (recorded absorption at 435 nm) yields an association constant (Ka) of 1.9×10^5 M^{-1}.

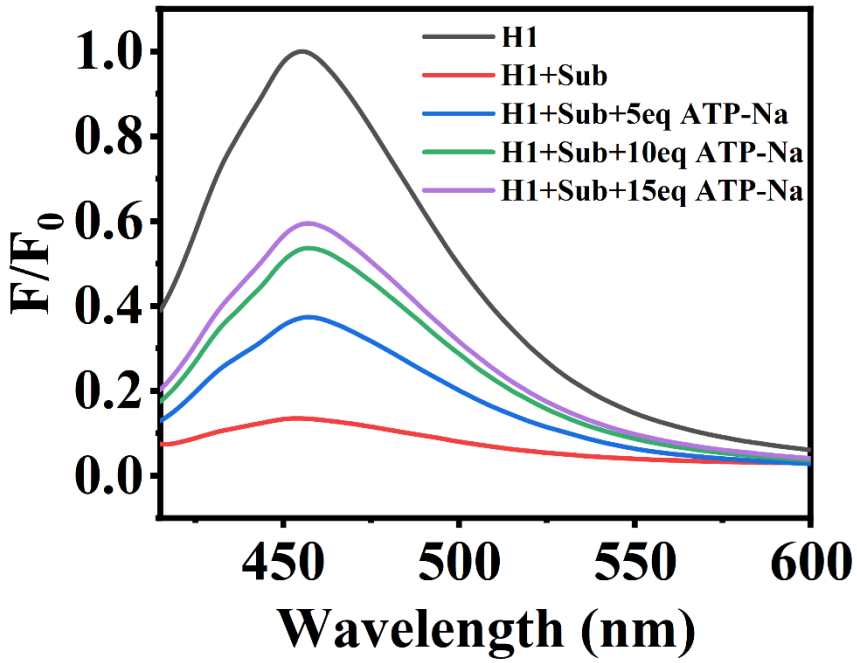

Figure S24. The emission spectra of H1 (0.01 mM) upon addition of 1a and ATP-Na.

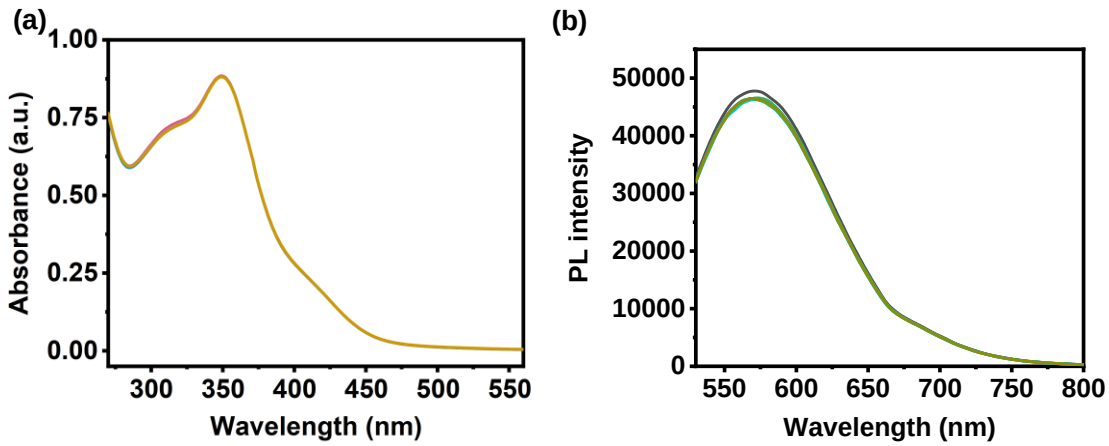

Figure S25. (a) UV-Vis titration of H2 (10 μM) upon the addition of 1a in CH_3CN. (b) Fluorescence emission spectra of H2 (10 μM) upon the addition of 1a in CH_3CN.

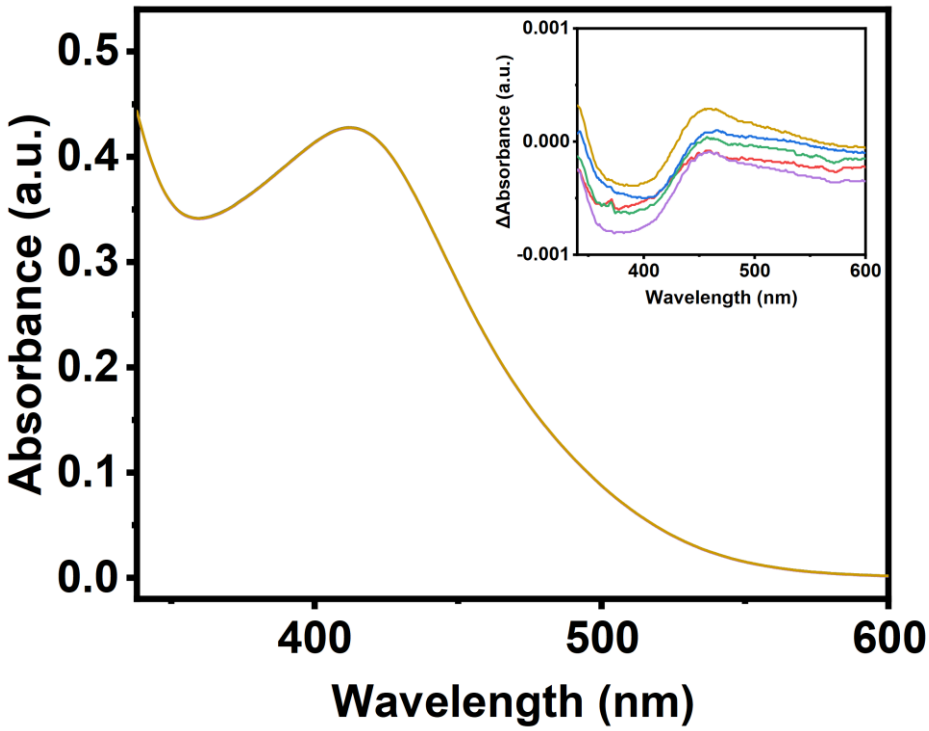

Figure S26. UV-Vis absorption spectra of **H1** upon the incremental addition of CH_3CN (in place of guest **1a**). The inset displays the corresponding differential absorption spectra.

Table S4: **Substrate scope of Reductive Amination**

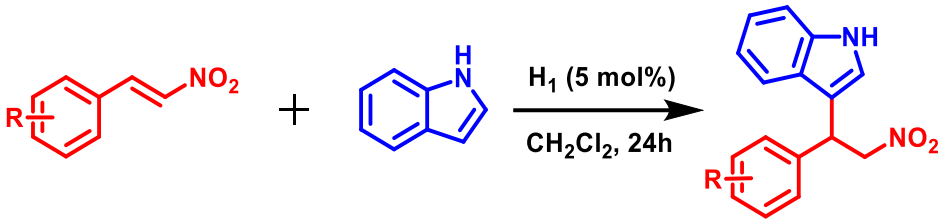

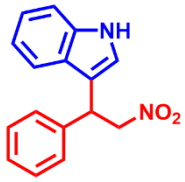

3a:63%

3b:53%

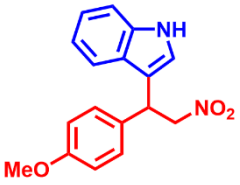

3c:56%

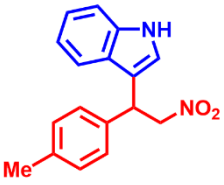

3d:58%

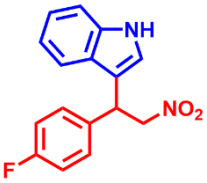

3e:62%

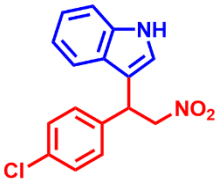

3f:62%

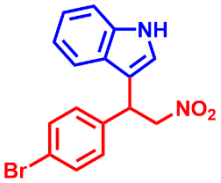

3g:61%

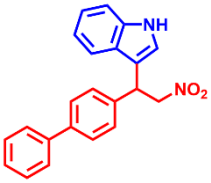

3h:36%

Standard conditions: substrate (0.05 mmol), indole (0.075 mmol), and H1 (5 mol%, 2.5 μmol) in CH_2Cl_2 (2 mL) at 60°C for 24 h. The yields were determined by ^1H NMR using 1,3,5-trimethoxybenzene as internal standard.

The equations and the derivation

For the linear fitting of the host-guest complex system[5]

For a 1:1 encapsulation process:

1. Equilibrium Assumption

Consider a host *H* and a guest *G* forming a host-guest inclusion complex HG_n with a binding stoichiometry of *1:n*:

$$H + nG \rightleftharpoons HG_n \quad (1)$$

The association constant *Ka* is defined as:

$$K_a = \frac{[HG_n]}{[H][G]^n}$$

Let the initial concentration of the host be $[H]_0$. Under the condition that the guest concentration is much larger than the host concentration ($[G] \gg [H]_0$), the free guest concentration *[G]* can be approximated as the total added guest concentration. Define the binding fraction x as:

$$x = \frac{[HG_n]}{[H]_0}$$

The free host concentration is then:

$$[H] = [H]_0 - [HG_n] = [H]_0(1 - x)$$

2. Expression for the Binding Fraction

Substituting these relationships into equation (1) gives:

$$K_a = \frac{x[H]_0}{(1-x)[H]_0[G]^n} = \frac{x}{(1-x)[G]^n}$$

Rearranging yields:

$$\frac{x}{1-x} = K_a[G]^n \quad (2)$$

3. Relationship Between Spectral Signal and Binding Fraction

In fluorescence or UV-Vis titration experiments, the measured signal *y* (fluorescence intensity or absorbance) can be considered as a linear combination of contributions from all species. Let y_0 be the initial signal in the absence of guest (corresponding to *x*=0), and y_L be the limiting signal when the guest is in large excess (corresponding to *x*=1). Assuming a linear relationship between the signal and the binding fraction:

$$y = y_0(1 - x) + y_L x \quad (3)$$

Solving for x gives:

$$x = \frac{y - y_0}{y_L - y_0} \quad (4)$$

and:

$$x = \frac{y_L - y}{y_L - y_0} \tag{5}$$

4. Linearization: The Hill-Plot Equation

Substituting equations (4) and (5) into equation (2):

$$\frac{y - y_0}{y_L - y} = K_a[G]^n \tag{6}$$

Taking the logarithm of both sides:

$$log\left(\frac{y - y_0}{y_L - y}\right) = log\, K_a + n\, log[G] \tag{7}$$

Equation (7) is the linear form of the Hill-plot.

4. Characterization Data for All Compounds

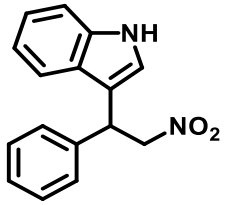

(3a)^{1}H NMR (500 MHz, DMSO-*d*$_6$) δ 11.06 (s, 1H), 7.51 (d, J = 7.9 Hz, 1H), 7.47-7.41 (m, 3H), 7.34 (d, J = 9.0 Hz, 1H), 7.29 (t, J = 7.6 Hz, 2H), 7.20 (t, J = 7.4 Hz, 1H), 7.09-7.03 (m, 1H), 6.97-6.91 (m, 1H), 5.39-5.27 (m, 2H), 5.05 (t, J = 8.3 Hz, 1H).

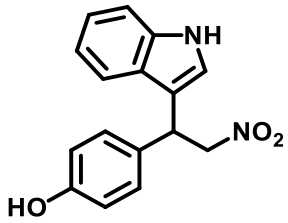

(3b)^{1}H NMR (500 MHz, DMSO-*d*$_6$) δ 11.00 (s, 1H), 9.30 (s, 1H), 7.46 (d, J = 7.9 Hz, 1H), 7.39-7.30 (m, 2H), 7.21 (d, J = 8.5 Hz, 2H), 7.09-7.02 (m, 1H), 6.96-6.90 (m, 1H), 6.66 (d, J = 8.7 Hz, 2H), 5.27 (dd, J = 12.8, 7.9 Hz, 1H), 5.18 (dd, J = 12.9, 8.6 Hz, 1H), 4.92 (t, J = 8.3 Hz, 1H).

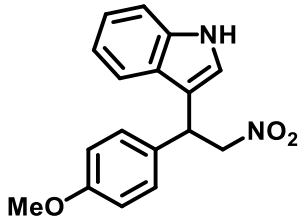

(3c) ^{1}H NMR (500 MHz, DMSO-*d*$_6$) δ 11.03 (s, 1H), 7.47 (d, J = 7.2 Hz, 1H), 7.40 (d, J = 2.5 Hz, 1H), 7.34 (t, J = 8.2 Hz, 3H), 7.06 (t, J = 7.6 Hz, 1H), 6.93 (t, J = 7.5 Hz, 1H), 6.84 (d, J = 8.7 Hz, 2H), 5.35-5.20 (m, 2H), 4.99 (t, J = 8.3 Hz, 1H), 3.69 (s, 3H).

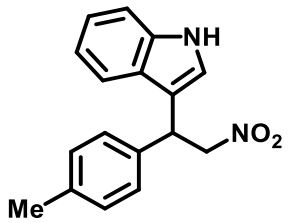

(3d) ^{1}H NMR (500 MHz, DMSO-*d*$_6$) δ 11.04 (s, 1H), 7.48 (d, J = 7.9 Hz, 1H), 7.40 (d, J = 2.7 Hz, 1H), 7.36-7.30 (m, 3H), 7.07 (dd, J = 18.8, 8.2 Hz, 3H), 6.94 (t, J = 7.5 Hz, 1H), 5.34-5.24 (m, 2H), 5.00 (t, J = 8.2 Hz, 1H), 2.23 (s, 3H).

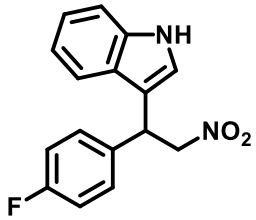

(3e) ^{1}H NMR (500 MHz, DMSO-*d*$_6$) δ 11.10 (s, 1H), 7.54-7.47 (m, 3H), 7.44 (d, J = 2.6 Hz, 1H), 7.35 (dd, J = 8.3, 5.1 Hz, 3H), 7.07 (t, J = 7.6 Hz, 1H), 6.95 (t, J = 7.5 Hz, 1H), 5.39-5.30 (m, 2H), 5.08 (t, J = 8.2 Hz, 1H).

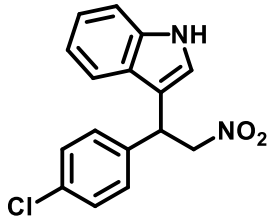

(3f) ^{1}H NMR (500 MHz, DMSO-*d*$_6$) δ 11.07 (s, 1H), 7.51 (d, J = 7.8 Hz, 1H), 7.49-7.42 (m, 3H), 7.37-7.26 (m, 3H), 7.06 (t, J = 7.6 Hz, 1H), 6.94 (t, J = 7.5 Hz, 1H), 5.40-5.27 (m, 2H), 5.05 (t, J = 8.3 Hz, 1H).

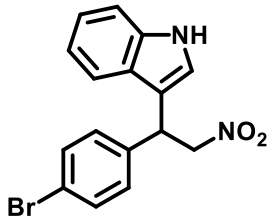

(3g)^{1}H NMR (500 MHz, DMSO-*d*$_6$) δ 11.09 (s, 1H), 7.49 (d, J = 8.4 Hz, 3H), 7.43 (d, J = 8.2 Hz, 3H), 7.35 (d, J = 8.2 Hz, 1H), 7.10-7.04 (m, 1H), 6.98-6.92 (m, 1H), 5.36-5.36 (m, 2H), 5.06 (t, J = 8.2 Hz, 1H).

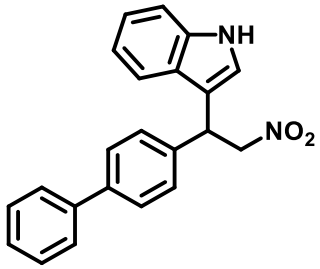

(3h)^{1}H NMR (500 MHz, DMSO-*d*$_6$) δ 11.08 (s, 1H), 7.61 (d, J = 7.2 Hz, 2H), 7.57 (q, J = 8.4 Hz, 5H), 7.48 (d, J = 2.6 Hz, 1H), 7.43 (t, J = 7.8 Hz, 2H), 7.34 (t, J = 8.3 Hz, 2H), 7.07 (t, J = 7.6 Hz, 1H), 6.96 (t, J = 7.5 Hz, 1H), 5.38 (d, J = 8.2 Hz, 2H), 5.11 (t, J = 8.3 Hz, 1H).

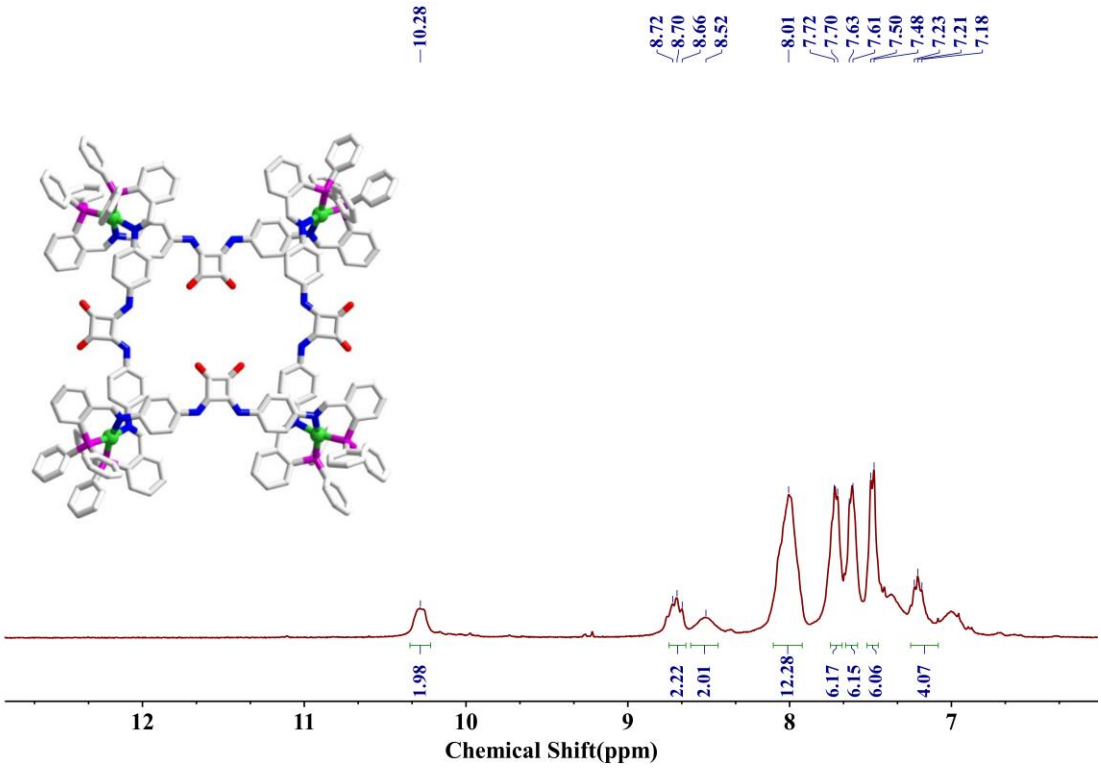

Figure S27. ^{1}H NMR (500 MHz, DMSO-*d6*) for compound H1.

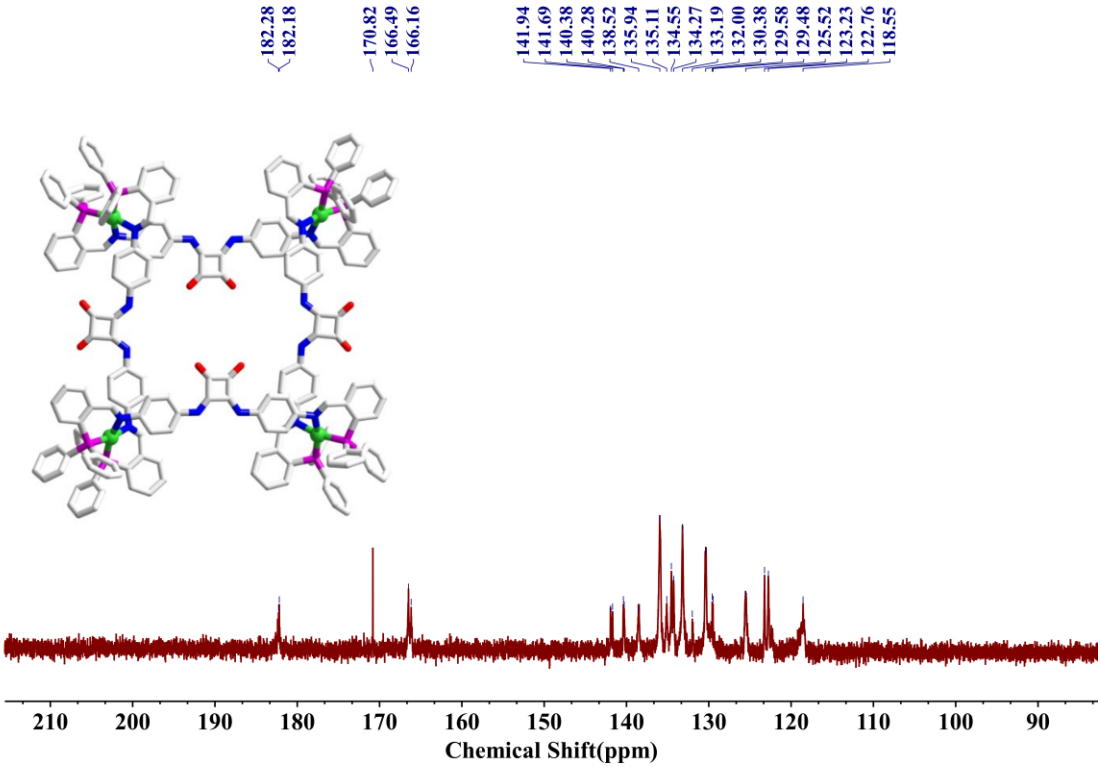

Figure S28. ^{13}C NMR (126 MHz, DMSO-*d6*) for compound H1.

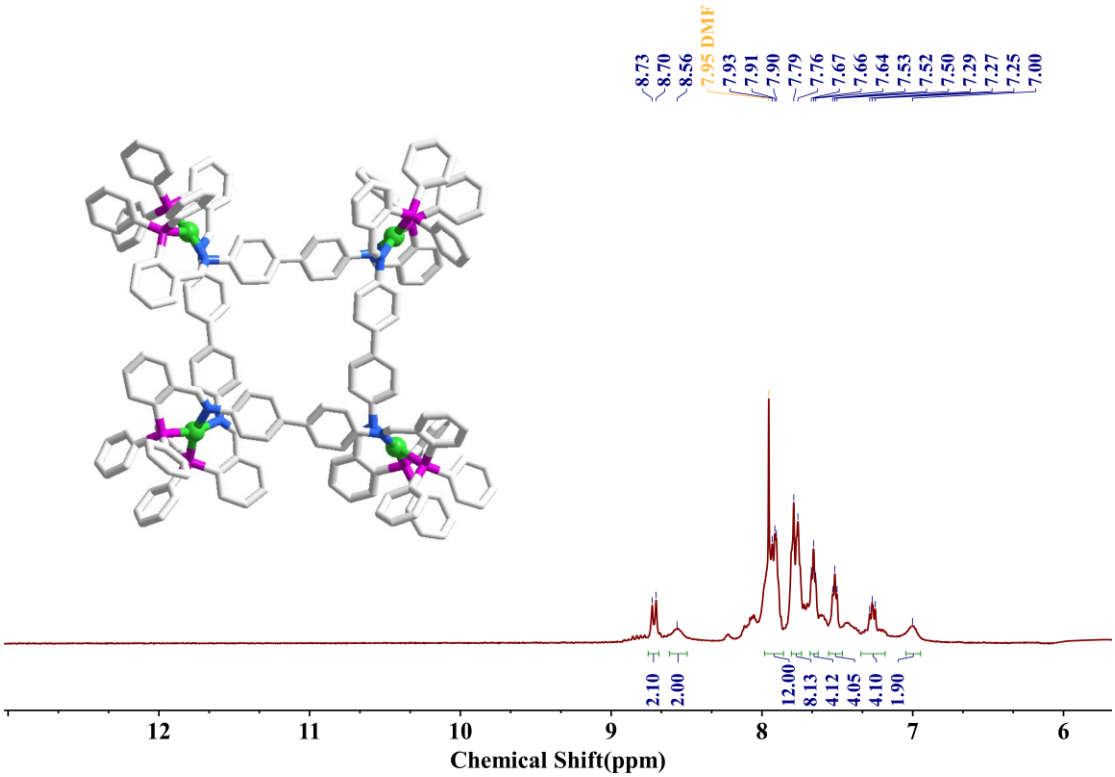

Figure S29. ^{1}H NMR (500 MHz, DMSO-*d6*) for compound H2.

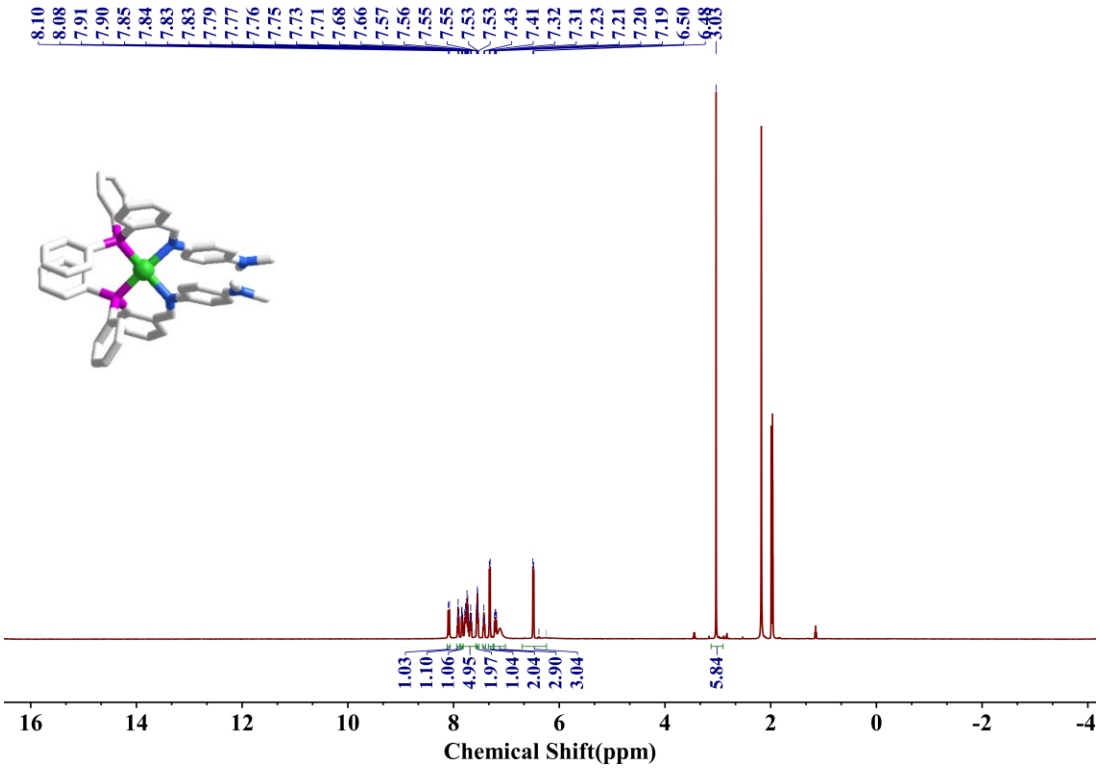

Figure S30. ^{1}H NMR (500 MHz, CD_3CN) for compound M1.

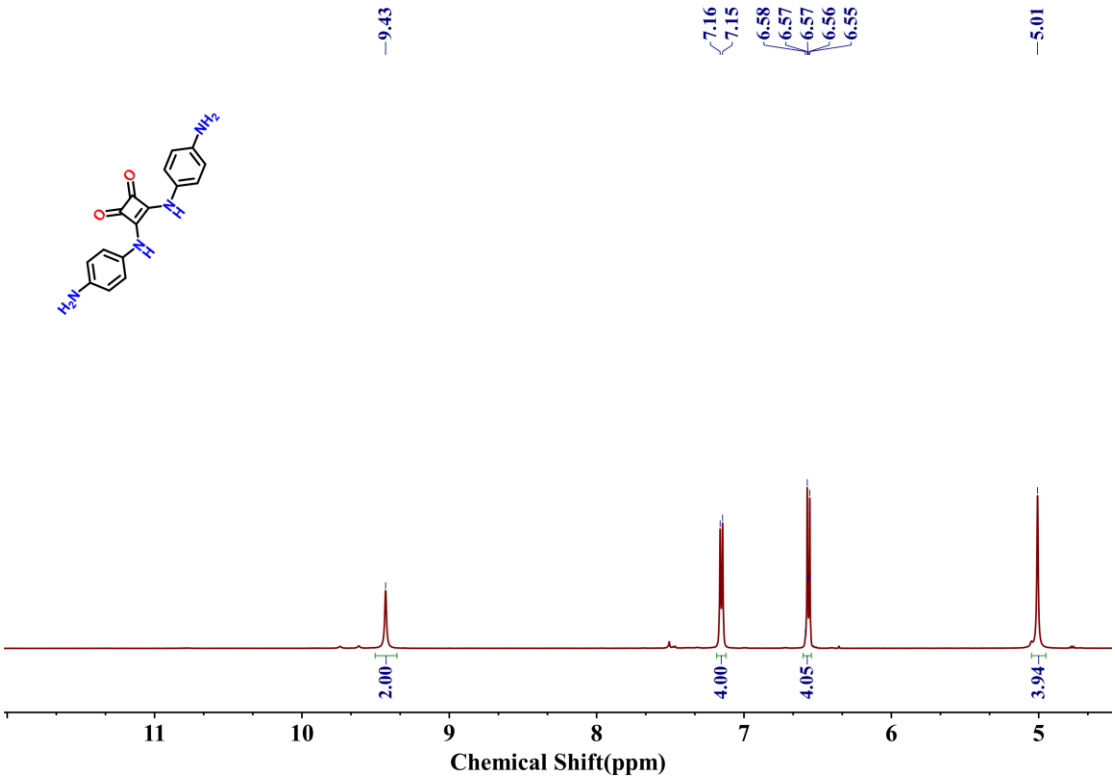

Figure S31. [1]H NMR (500 MHz, DMSO-*d6*) for compound L.

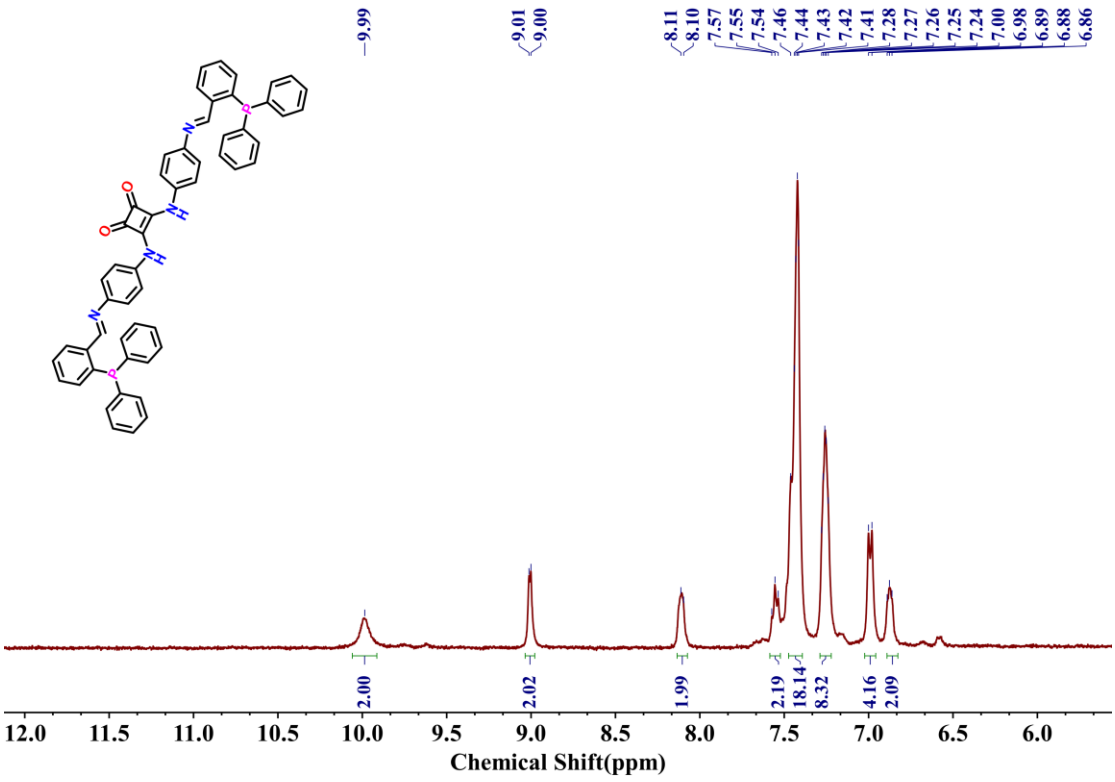

Figure S32. [1]H NMR (400 MHz, DMSO-*d6*) for compound L1.

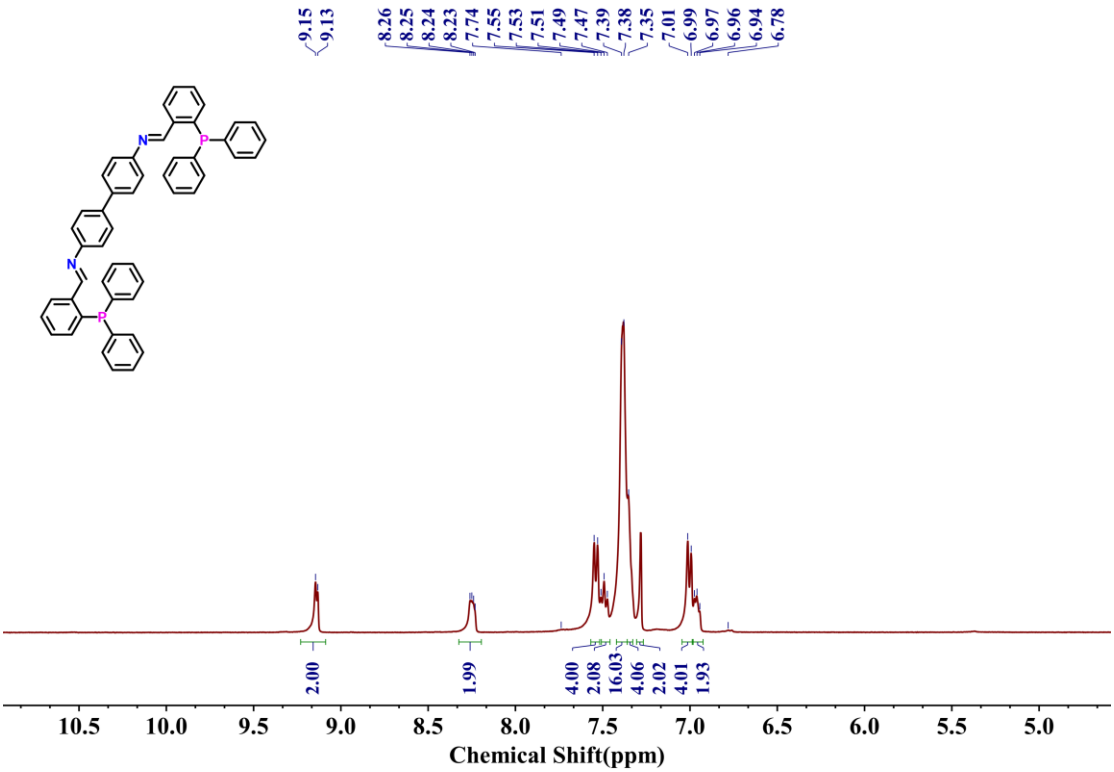

Figure S33. ^{1}H NMR (400 MHz, $CDCl_3$) for compound L2.

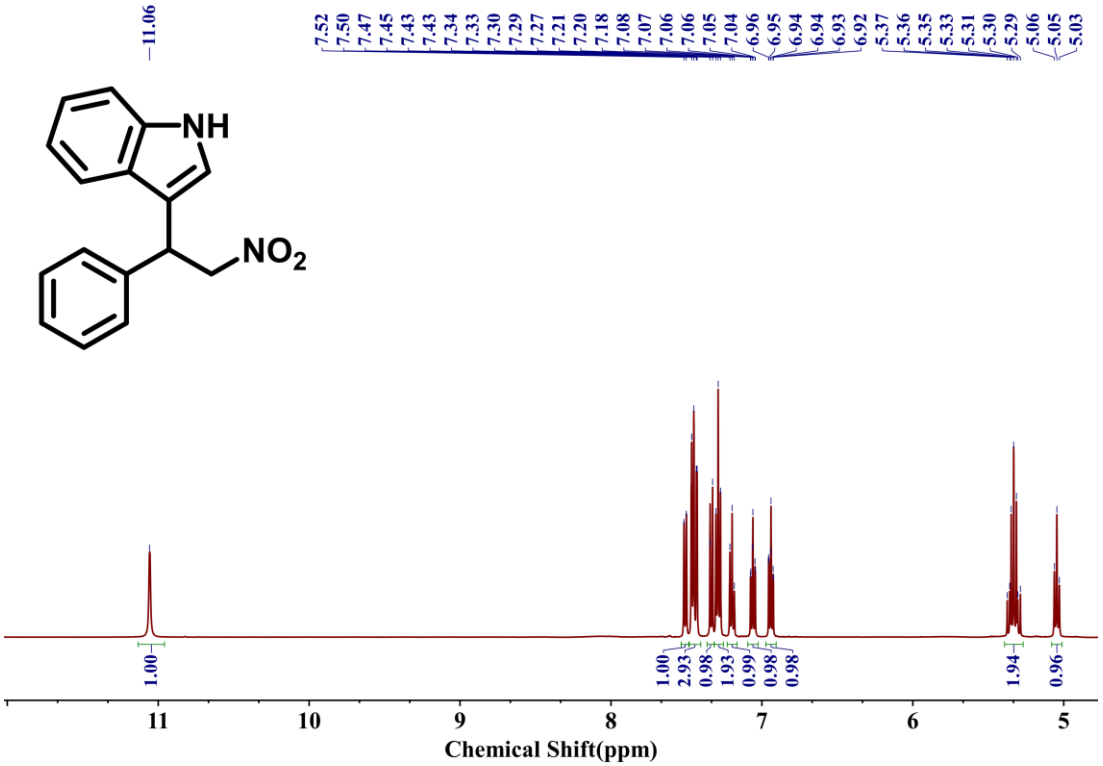

Figure S34. [1]H NMR (500 MHz, DMSO-*d6*) for compound 1a.

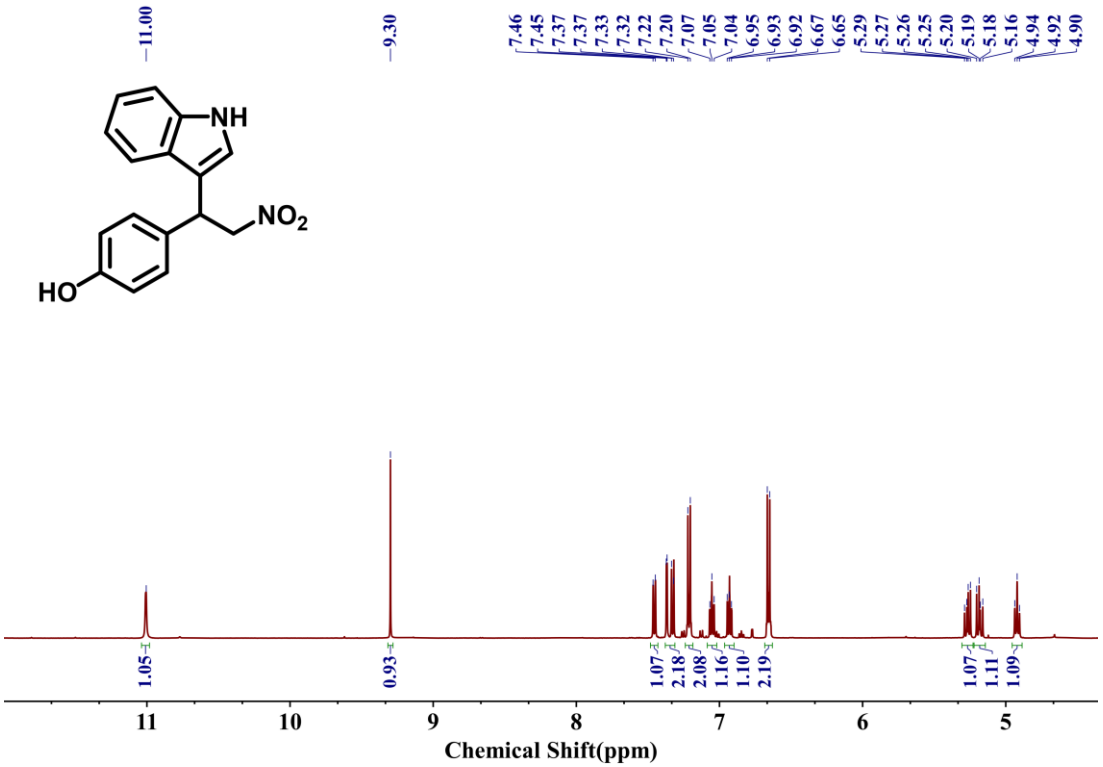

Figure S35. [1]H NMR (500 MHz, DMSO-*d6*) for compound 1b.

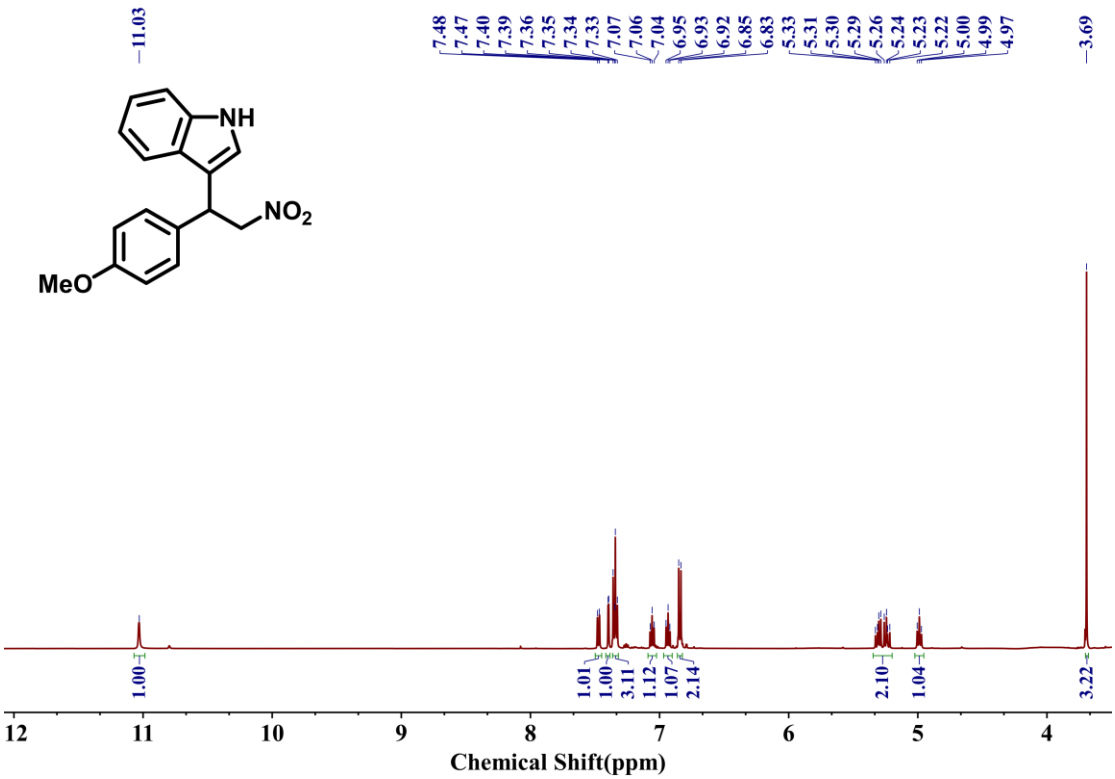

Figure S36. [1]H NMR (500 MHz, DMSO-*d6*) for compound 1c.

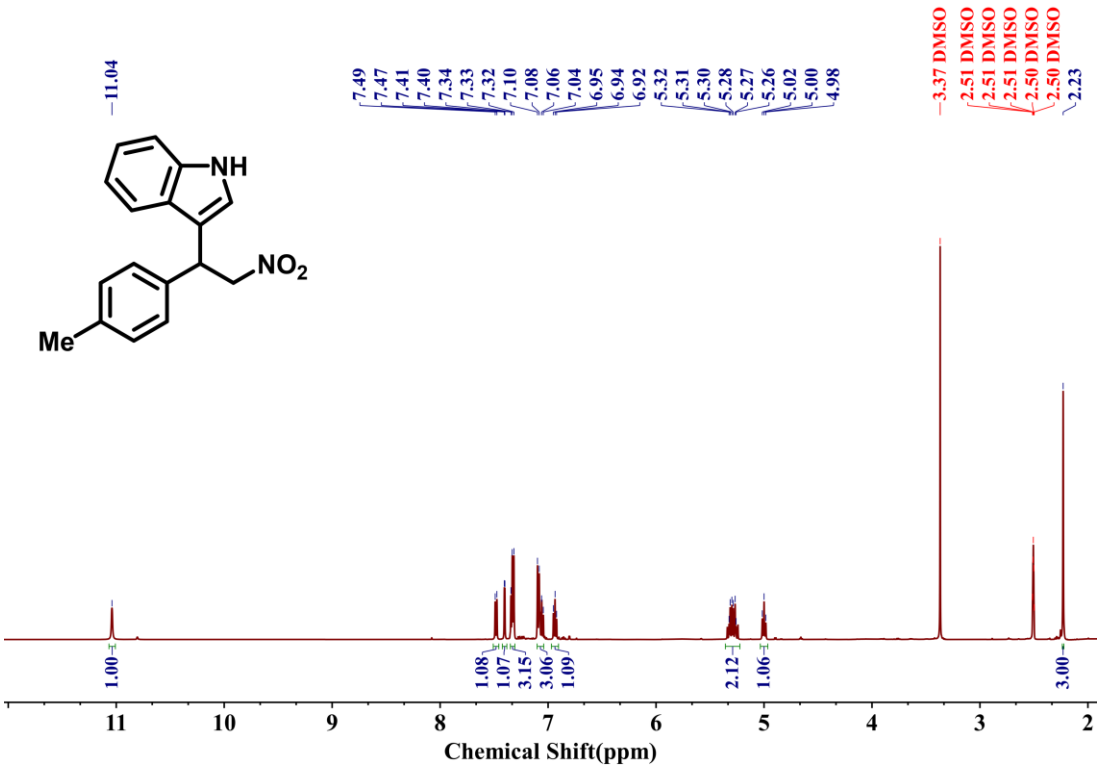

Figure S37. [1]H NMR (500 MHz, DMSO-*d6*) for compound 1d.

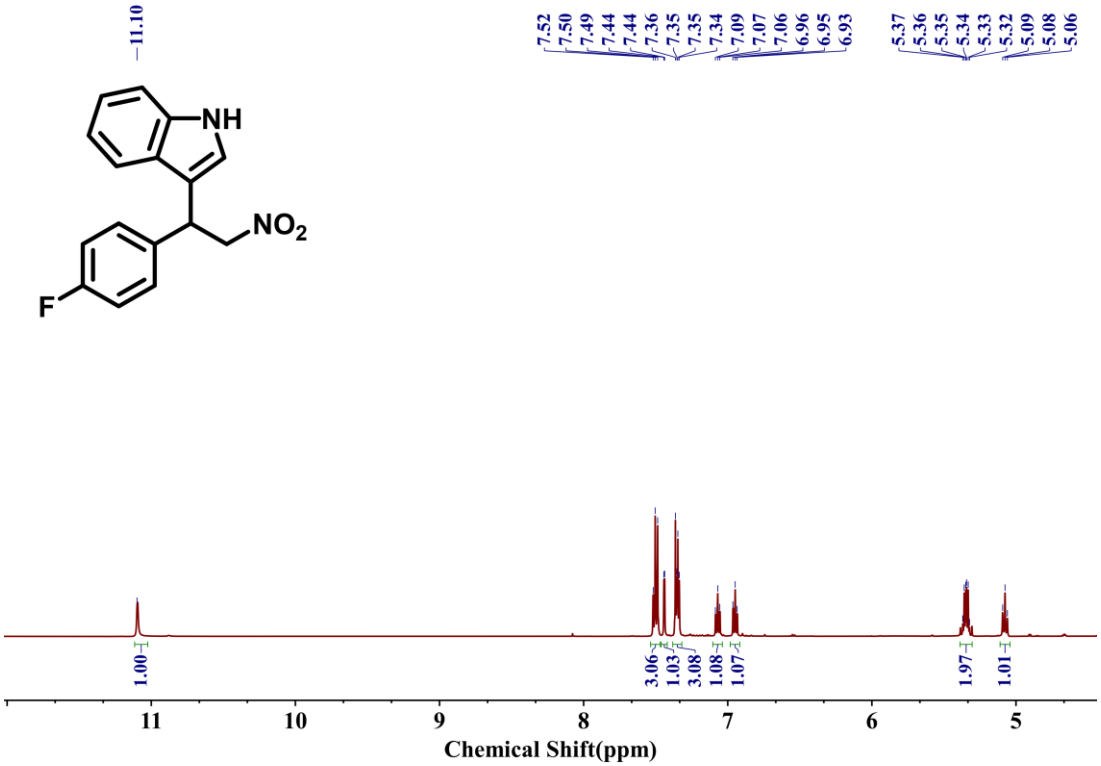

Figure S38. ^{1}H NMR (500 MHz, DMSO-*d6*) for compound 1e.

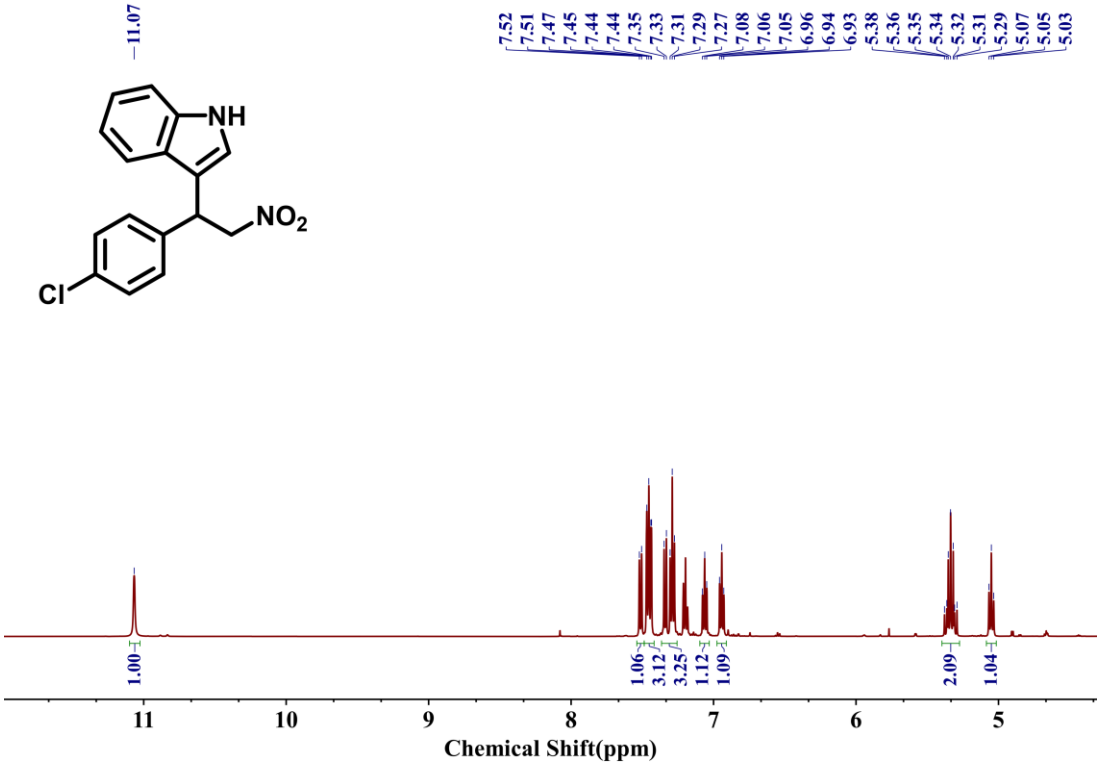

Figure S39. ^{1}H NMR (500 MHz, DMSO-*d6*) for compound 1f.

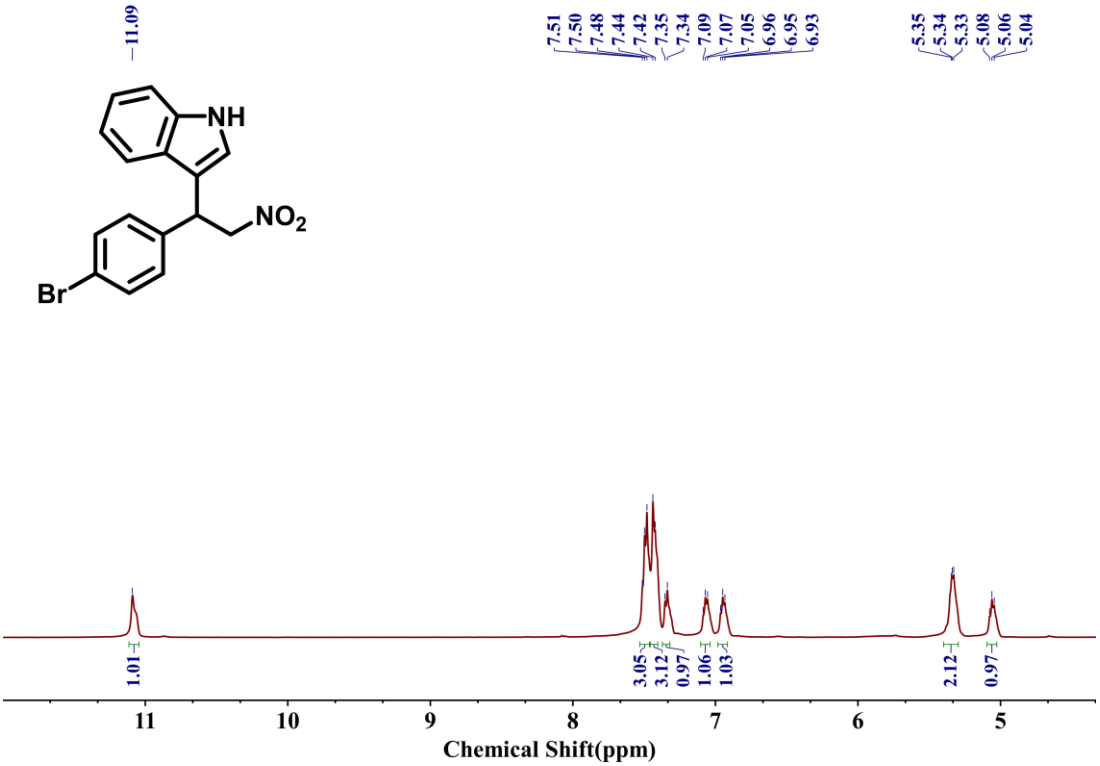

Figure S40. ^{1}H NMR (500 MHz, DMSO-*d6*) for compound 1g.

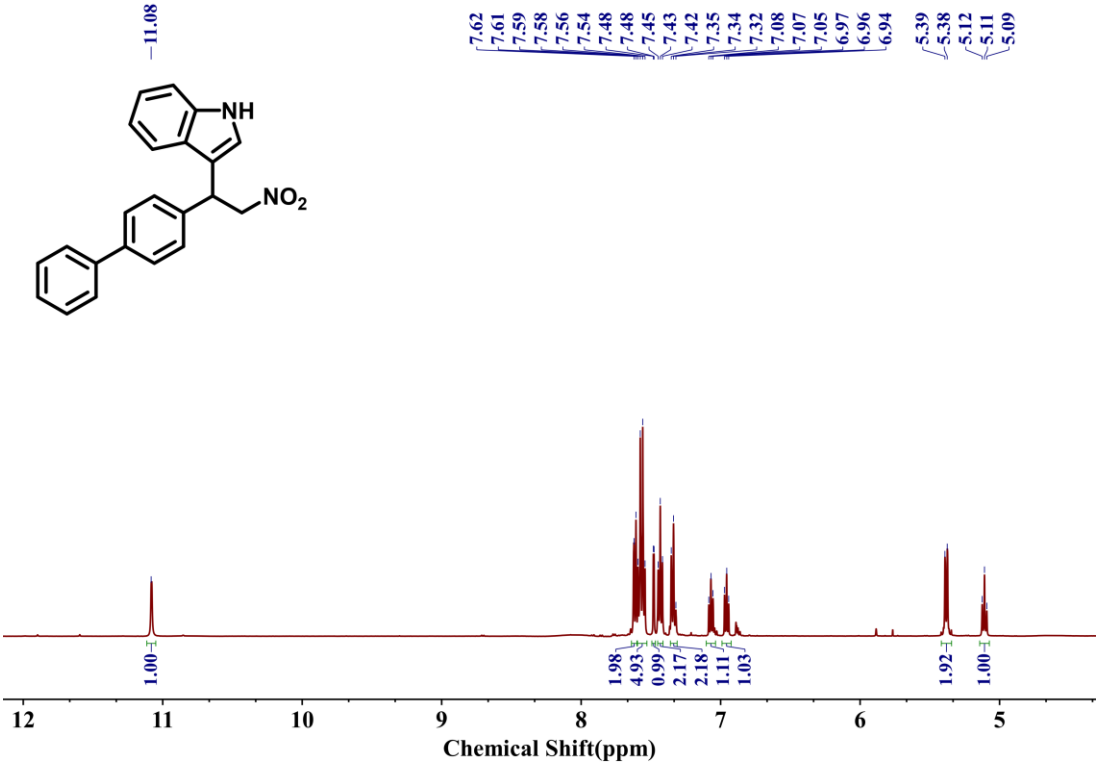

Figure S41. ^{1}H NMR (500 MHz, DMSO-*d6*) for compound 1h.

References

1. X. Li, Z. F. Wang, J. X. Sun, J. Gao, Y. Zhao, P. Cheng, B. Aguila, S. Q. Ma, Y. Chen and Z. J. Zhang, *Chem. Commun*, 2019, **55**, 5423-5426.
2. L. Krause, R. Herbst-Irmer, G. M. Sheldrick and D. Stalke, J. Appl. *Crystallogr.*, 2015, **48**, 3-10.
3. G. M. Sheldrick, *Acta Crystallogr. Sect. C*, 2015, **71**, 3-8.
4. A. L. Spek, *Acta Crystallogr. Sect. C*, 2015, **71**, 9-18.
5. J. W. Wei, L. Zhao, Y. Zhang, G. Han, C. He, C. Wang and C. Y. Duan, *J. Am. Chem. Soc.*, 2023, **145**, 6719-6729.